



Fourteen months of on-line measurements of the non-refractory submicron aerosol at the Jungfraujoch (3580 m a.s.l.) – chemical composition, origins and organic aerosol sources

R. Fröhlich¹, M. J. Cubison², J. G. Slowik¹, N. Bukowiecki¹, F. Canonaco¹, P. L. Croteau³, M. Gysel¹, S. Henne⁴, E. Herrmann¹, J. T. Jayne³, M. Steinbacher⁴, D. R. Worsnop³, U. Baltensperger¹, and A. S. H. Prévôt¹

¹Laboratory of Atmospheric Chemistry, Paul Scherrer Institute, Villigen PSI, Switzerland

²Tofwerk AG, Thun, Switzerland

³Aerodyne Research Inc., Billerica, Massachusetts, USA

⁴Laboratory for Air Pollution/Environmental Technology, Empa, Swiss Federal Laboratories for Materials Science and Technology, Dübendorf, Switzerland

Correspondence to: A. S. H. Prévôt (andre.prevot@psi.ch)

Received: 26 May 2015 – Published in Atmos. Chem. Phys. Discuss.: 7 July 2015

Revised: 7 September 2015 – Accepted: 28 September 2015 – Published: 14 October 2015

Abstract. Chemically resolved (organic, nitrate, sulfate, ammonium) data of non-refractory submicron (NR-PM₁) aerosol from the first long-term deployment (27 July 2012 to 02 October 2013) of a time-of-flight aerosol chemical speciation monitor (ToF-ACSM) at the Swiss high-altitude site Jungfraujoch (JFJ; 3580 m a.s.l.) are presented. Besides total mass loadings, diurnal variations and relative species contributions during the different meteorological seasons, geographical origin and sources of organic aerosol (OA) are discussed. Backward transport simulations show that the highest (especially sulfate) concentrations of NR-PM₁ were measured in air masses advected to the station from regions south of the JFJ, while lowest concentrations were seen from western regions. OA source apportionment for each season was performed using the Source Finder (SoFi) interface for the multilinear engine (ME-2). OA was dominated in all seasons by oxygenated OA (OOA, 71–88 %), with lesser contributions from local tourism-related activities (7–12 %) and hydrocarbon-like OA related to regional vertical transport (3–9 %). In summer the OOA can be separated into a background low-volatility OA (LV-OOA I, possibly associated with long-range transport) and a slightly less oxidised low-volatility OA (LV-OOA II) associated with regional vertical transport. Wood burning-related OA associated with regional transport was detected during the whole winter 2012/2013 and during rare events in summer 2013, in the latter case

attributed to small-scale transport for the surrounding valleys. Additionally, the data were divided into periods with free tropospheric (FT) conditions and periods with planetary boundary layer (PBL) influence, enabling the assessment of the composition for each. Most nitrate and part of the OA are injected from the regional PBL, while sulfate is mainly produced in the FT. The south/north gradient of sulfate is also pronounced in FT air masses (sulfate mass fraction from the south: 45 %; from the north: 29 %). Furthermore, a detailed investigation of specific marker fragments of the OA spectra (f_{43} , f_{44} , f_{55} , f_{57} , f_{60}) showed different degrees of ageing depending on season.

1 Introduction

Many environmental topics which are becoming increasingly important in the future are closely linked to aerosols, e.g. climate change on global (Charlson et al., 1992; Lohmann and Feichter, 2005; Boucher et al., 2013) and regional scales (Ramanathan et al., 2001; Stott, 2003; Shindell and Faluvegi, 2009), or impacts on human health (Seaton et al., 1995; Laden et al., 2000; Cohen et al., 2005; Pope and Dockery, 2006) and Earth's ecosystem (Mahowald, 2011). Therefore a good knowledge of aerosol chemical and physical properties in the atmosphere is an essential scientific task. In

situ measurements of these properties provide the basis for a deeper understanding of the aerosol influence on the topics mentioned above.

Knowledge of the aerosol concentrations and properties in the lower FT is important due to its impact on cloud formation and to validate model results from the FT. The high-altitude research station on the Jungfrauoch (JFJ) at 3580 m a.s.l. in the Swiss Alps allows the investigation of free tropospheric aerosol year round due to its elevated location. Nevertheless, vertical transport of polluted air masses from the planetary boundary layer (PBL) is observed occasionally especially in summer (see Lugauer et al., 1998; Henne et al., 2004, 2010). However, suitable approaches have been applied in the past to discriminate between PBL-influenced conditions and free tropospheric air masses (see Sect. 2.5). Due to its well-developed infrastructure and unique location many decades of scientific measurements of gas-phase constituents (Zander et al., 2008; Pandey Deolal et al., 2012), meteorology (Appenzeller et al., 2008) and atmospheric aerosols (Baltensperger et al., 1997; Collaud Coen et al., 2007; Cozic et al., 2008; Bukowiecki et al., 2015) have been performed there. Given the absence of local vegetation and small scale of local emissions, the JFJ is an ideal location for the measurement of pollution arriving from all over Europe (Reimann et al., 2008; Uglietti et al., 2011).

An important property of atmospheric aerosol particles is their chemical composition providing insight into their origin and chemical evolution pathways. Aerosol mass spectrometry provides a tool for measuring the chemical composition with high-time resolution as opposed to the collection of filter samples, which are often prone to sampling artefacts. The application of the aerosol mass spectrometer (Jayne et al., 2000, AMS, Aerodyne Research Inc., Billerica, MA, USA) has produced a large database of aerosol chemical composition around the planet (see e.g. Zhang et al., 2007; Jimenez et al., 2009; Crippa et al., 2014). However, because of the complexity and cost of the instrument, most AMS measurements cover only a few days to weeks of sampling. Exceptions are a 1-year continuous AMS measurement in London by Young et al. (2015) and a 3-year data set from Mace Head by Ovadnevaite et al. (2014).

To facilitate long-term mass spectrometric measurements, the aerosol chemical speciation monitor (Ng et al., 2011c, ACSM) was developed. Long-term measurements are essential to capture long-term trends, inter-season variations or other effects taking place on longer timescales. Furthermore, increasing data coverage allows for a more reliable determination of the typical aerosol conditions at a specific site. The ACSM provides a valuable and robust tool for measuring chemical composition of submicron aerosol with time resolutions on the order of minutes to hours on a long-term basis. Several long-term and medium-term ACSM data sets have been presented in the literature: 2 years near Paris (France) (Petit et al., 2015), 1.5 years in central Oklahoma (Parworth et al., 2015), 1 year in Zurich (Switzerland) (Canonaco et al.,

2013, 2015), near Johannesburg (South Africa) (Tiitta et al., 2014; Vakkari et al., 2014), near Barcelona (Spain) (Ripoll et al., 2015; Minguillón et al., 2015), and in the Southeastern United States (Budisulistiorini et al., 2015), between 1.5 and 3.5 months in Tijuana (Mexico) (Takahama et al., 2013), on Crete (Greece) (Bougiatioti et al., 2014), in Atlanta (USA) (Budisulistiorini et al., 2013), in Beijing (China) (Sun et al., 2012) and in Santiago de Chile (Chile) (Carbone et al., 2013). In addition, a large database of long-term ACSM data sets (including the data set presented in this manuscript) will be made available in the framework of the European ACTRIS (Aerosols, Clouds, and Trace gases Research Infrastructure) project (see stations overview at <http://www.psi.ch/acsm-stations/acsm-and-emep-stations>) via the EBAS database hosted by the Norwegian Institute for Air Research (NILU, <http://ebas.nilu.no/>).

In the present manuscript 14 months of data from the first long-term deployment of a time-of-flight aerosol chemical speciation monitor (ToF-ACSM, Fröhlich et al., 2013) are presented. The ToF-ACSM provides the advantage of increased sensitivity compared to the ACSM version using a quadrupole mass spectrometer, making it more suitable for remote locations with low expected mass concentrations like the JFJ. The high time resolution of 10 min allows for a year-round detailed analysis of chemical composition of aerosol, which to our knowledge to date is unique for the high Alpine environment and was made possible only by the development of the ToF-ACSM. Diurnal as well as seasonal cycles are discussed together with the influence of injected air from the PBL and the influence of different source regions on the chemical composition. Furthermore, a closer look at the chemical evolution of the organic aerosol fraction and its sources is presented.

2 Methods

2.1 Measurement site

The Sphinx observatory is part of the High Alpine Research Station Jungfrauoch, which is integrated into several measurement networks: amongst others there are the international Global Atmosphere Watch (GAW) programme of the World Meteorological Organisation (WMO), the Swiss National Monitoring Network for Air Pollutants (NABEL) and the European ACTRIS infrastructure project. It is located at an elevation of 3580 m a.s.l. (07°59'02" E, 46°32'53" N) on an exposed rock formation on the saddle between the two mountains Jungfrau (4158 m a.s.l.) and Mönch (4107 m a.s.l.). The surrounding topography leads to a channelling of local winds in north-westerly or south-easterly directions (see e.g. Hammer et al., 2014). In the north-west the terrain descends steeply towards the Bernese Oberland with Lake Thun and Lake Brienz, while in the opposite (south-east) direction the descent is less steep over the Valaisian

Great Aletsch glacier and the Rhône Valley. While the upper two floors of the Sphinx observatory are reserved solely for scientific purposes the lower levels are accessible to tourists who are the only small but ever growing (866 000 visitors in 2014) source of local pollution. Monthly average outside temperatures are below freezing year round. Appenzeller et al. (2008) reported about 10–20 annual days with minimum daytime temperatures above 0 °C, with an increasing trend (50 % increase for the investigated period between 1961 and 2005).

Measurements took place between 27 July 2012 and 2 October 2013, spanning all seasons (see Fig. 1a and b) and totalling more than one year. Recorded concentrations are in agreement with previous studies investigating chemical composition at the JFJ, making the findings representative of the JFJ aerosol. A recent review compiling the results of 20 years of aerosol measurements at the JFJ was published by Bukowiecki et al. (2015). All data are reported in UTC, which is local time minus 1 h in winter and local time minus 2 h in summer (daylight saving time), respectively.

2.2 Instrumentation

The ToF-ACSM (Aerodyne Inc., Billerica, MA, USA and Tofwerk AG, Thun, BE, Switzerland) which is described in detail in Fröhlich et al. (2013), is applied for the chemical composition measurements. Like the quadrupole ACSM (Q-ACSM, Ng et al., 2011c), the ToF-ACSM is based on Aerodyne AMS technology but is smaller, less costly, and optimised for long-term deployment with minimal maintenance. In comparison to the Q-ACSM, the ToF-ACSM features improved mass-to-charge resolution ($\frac{M}{\Delta M} = 500$, enabling separation of some isobaric components in the mass spectrum using peak fitting if desired) and, more importantly for deployments at remote sites, improved sensitivity. Additionally, the ToF-ACSM provides the possibility to span a larger m/z range (up to $m/z \approx 300$ Th) than the Q-ACSM where the technical limitation lies around m/z 150. At the JFJ, data were averaged to 10 min (corresponding to an organic aerosol detection limit of 63 ng m^{-3} according to Fröhlich et al., 2013).

The deployment at the JFJ represented the first field test of the ToF-ACSM instrument. Optimisation and upgrading of the instrument and software continued throughout the deployment, especially during the first half of the year, resulting in occasional breaks in operation (cf. Fig. 1a). Even including these planned downtimes, the ToF-ACSM measured for 73 % of the entire deployment and 97 % during the last 5 months (after the final configuration was reached).

The ToF-ACSM provides quantitative mass spectra of non-refractory (NR) submicron (PM₁) aerosol. The operational principles are described in detail elsewhere (Fröhlich et al., 2013) and summarised here in four key steps: separation of particles from gas-phase molecules, flash vaporisation, ionisation of the resulting vapour molecules, and sort-

ing of the consequent ions by time-of-flight mass spectrometry. Separation, focusing and PM₁ size cut of the particles is achieved by combination of an aerodynamic lens and a skimmer cone. Because of the low ambient atmospheric pressures at the JFJ (average 655 hPa) the instrument inlet was modified by replacing the standard critical orifice ($d = 100 \mu\text{m}$) with an orifice that has a diameter of $d = 130 \mu\text{m}$. This keeps the inlet mass flow rates comparable to those obtained during standard operation at lower elevations. Flash vaporisation of non-refractory species takes place at $T = 600^\circ\text{C}$ on a heated porous tungsten plate and ionisation is performed by electron ionisation at $E_{\text{kin}} = 70 \text{ eV}$.

Ion fragments are attributed to the main constituents of aerosol particles, organics, nitrate (NO_3^-), sulfate (SO_4^{2-}), ammonium (NH_4^+) and chloride (Cl^-) according to the fragmentation table-based analysis developed by Allan et al. (2004). At the JFJ, chloride concentrations were always below the 10 min detection limit of the ToF-ACSM (4 ng m^{-3}) and hence chloride is omitted in the following discussion.

All necessary calibrations as detailed in Fröhlich et al. (2013) (signal-to-mass (mIE), NO_3^- relative ionisation efficiency (RIE) of sulfate and ammonium, flow rate) were performed on a monthly to bimonthly schedule. Calibrated RIE values were 3.2 ± 0.4 for NH_4^+ and 0.6 ± 0.1 for SO_4^{2-} . The mean values were applied throughout the data set. For organic molecules, the standard RIE of 1.4 was applied (Alfarra et al., 2004; Canagaratna et al., 2007).

Previous short-term measurements with ACSM and AMS at the JFJ showed a particle collection efficiency (CE) close to unity (Lanz et al., 2010; Jurányi et al., 2010; Fröhlich et al., 2013). The same CE = 1 was applied to the data of this study. This expectation was confirmed by plotting total mass concentration measured with the ToF-ACSM plus equivalent black carbon (eBC) from optical absorption measurements vs. the total mass estimated from a scanning mobility particle sizer (SMPS; for a detailed set-up description, see Jurányi et al., 2011; Herrmann et al., 2015), which resulted in distributions around the 1 : 1 line during all seasons (see Fig. S1 in the Supplement). For that analysis, periods with high concentrations of refractory particles (e.g. Saharan dust events – see Sect. 2.6 for method of separation – or construction work) were excluded from the correlation. To convert SMPS number size distributions into mass, a density ρ_{part} was estimated according to the relative densities of the main species measured by the ToF-ACSM at the JFJ: SO_4^{2-} and organics (together almost always > 80 % of total PM₁). Densities of 1.8 g cm^{-3} for sulfate and 1.3 g cm^{-3} for organics (experimentally determined by Cross et al., 2007) were applied. The high CE close to unity is uncommon as typically a CE around 0.5 is reported for AMS/ACSM instruments because a fraction of NR particles is lost due to bounce off the vaporiser before flash vaporisation. According to Matthew et al. (2008) this bounce depends on particle phase and is reduced if particles are either wet, acidic or containing high fractions of

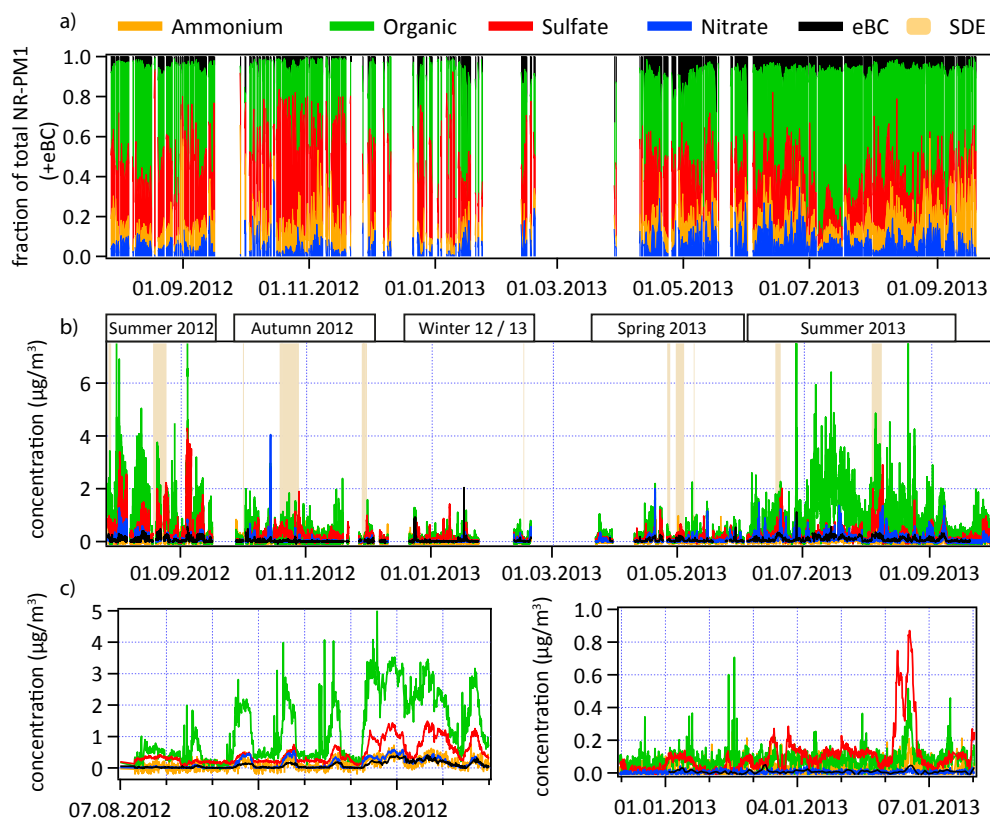


Figure 1. (a) Time series of relative organic (green), sulfate (red), nitrate (blue), and ammonium (orange) contributions to the total PM₁ aerosol measured by the ToF-ACSM and the eBC (black) concentration time series measured by the aethalometer from 27 July 2012 to 02 October 2013. (b) Same as (a) in absolute concentrations ($\mu\text{g m}^{-3}$). Saharan dust events (SDE) are highlighted in light brown. On top of (b) the periods used in the following seasonal analyses are identified. Gaps between seasons are caused by gaps in the data. (c) Left: mass concentrations in $\mu\text{g m}^{-3}$ during a typical summer period (7 August 2012 00:00 to 15 August 2012 00:00); right: mass concentrations in $\mu\text{g m}^{-3}$ during a typical winter period (01 January 2013, 00:00 to 08 January 2013, 00:00). Note the different y scales of the two plots in (c). Times are given in UTC.

nitrate. All three conditions are not fulfilled at the JFJ. The reason for the discrepancy is still unknown but it is noted that compared to other atmospheric measurement sites the JFJ exhibits extreme ambient conditions (pressure, temperature).

The ToF-ACSM was connected to the total inlet (see e.g. Weingartner et al., 1999; Henning et al., 2003) which is also used for the aerosol monitoring instrumentation of the GAW programme on site. Heating of the inlet to indoor temperatures ($T = 25^\circ\text{C}$) avoids build-up of ice and ensures dry aerosol without the use of additional drying equipment due to the always low outside temperatures at the JFJ (annual mean temperature: $T_{\text{mean}} = -7^\circ\text{C}$, highest monthly mean temperature in July: $T_{\text{mean, July}} = -1.2^\circ\text{C}$). A bypass flow of $50\text{ cm}^3\text{ s}^{-1}$ in addition to the $2.4\text{ cm}^3\text{ s}^{-1}$ flow of the ToF-ACSM makes particle losses in the inlet line ($d = 5\text{ mm}$; $l \approx 2\text{ m}$) negligible.

Furthermore, data from a nephelometer (Model 3563, TSI inc., Shoreview, MN, USA), a condensation particle counter (CPC, Model 3772, TSI inc., Shoreview, MN, USA), and an

aethalometer (AE31, Magee Scientific, Berkeley, CA, USA) operated at the JFJ in the framework of the GAW activities were used in the context of this study. The default mass attenuation cross section for aerosol on the filter matrix (MAC_{atm} value) from the AE31 manual of $16.6\text{ m}^2\text{ g}^{-1}$ at 880 nm (no loading correction) was applied to determine eBC. MAC_{atm} accounts for instrumental error and optical properties of the aerosol. The latter varies between sites and aerosol type (for details see Weingartner et al. (2003) and Zanatta et al. (2015)). For the determination of the boundary layer influence on the air masses at the JFJ, data from a ^{222}Rn analyser built by the Australian Nuclear Science and Technology Organisation (ANSTO) and operated by the University of Basel (for more details see Griffiths et al., 2014), NO_y data measured by chemiluminescence (CraNO_x , Eco Physics, Dürnten, Switzerland, Pandey Deolal et al., 2012) and CO data from a cavity ring-down spectrometer (model G2401, Picarro Inc, Santa Clara, CA, USA, Zellweger et al., 2012) of the NABEL network were used.

2.3 Bilinear factor analysis with the multilinear engine (ME-2)

Positive matrix factorisation (PMF, Paatero and Tapper, 1994; Paatero, 1997) facilitates disentanglement of bulk mass spectral time series into several contributing factors by minimisation of the quantity Q , consisting of the sum of the squares of the error-weighted residuals of the model. Especially for the organic part of the aerosol mass spectra recorded with AMS/ACSM instruments this method is very successful (Lanz et al., 2007) and has been applied to a great number of studies around the world (Zhang et al., 2011). In conventional PMF analyses, rotational ambiguity coupled with limited rotational controls can impede clean factor resolution. In contrast, the multilinear engine implementation (ME-2, Paatero, 1999; Paatero and Hopke, 2009) enables efficient exploration of the entire solution space by the application of specifically designed penalties or restrictions to mathematically viable but physically unrealistic or ambiguous solutions. A simple approach utilises the so-called a value (Lanz et al., 2008; Brown et al., 2012; Canonaco et al., 2013; Crippa et al., 2014). Here a priori information is introduced by fixing one or more anchor spectra from previous campaigns/analyses with varying degree of freedom. The freedom is regulated with the a value which can vary between 0 and 1 and stands for the percentage each m/z signal of the final solution spectra may differ from the anchor. 0 means no deviation allowed; 1 means 100 % deviation allowed.

The source finder (SoFi, Canonaco et al., 2013) tool version 4.9 for Igor Pro (WaveMetrics Inc., Lake Oswego, OR) was used for ME-2 input preparation and result analysis.

2.4 Back dispersion (BD) clustering

For the full measurement period, the history of air masses arriving at the JFJ was calculated using backward simulations of the Lagrangian particle dispersion model FLEXPART (v9.01, Stohl et al., 2005). Taking into account mean flow, deep convection, and turbulence, the model calculated the backward trajectories (10 days) of 50 000 particles released every 3 h at the location of the JFJ. The model was driven off-line with meteorological data from the European Centre for Medium Range Weather Forecast (ECMWF) at a vertical resolution of 91 levels (138 levels after 25 June 2013) and a horizontal resolution of $0.2^\circ \times 0.2^\circ$ for the Alpine area (rest: $1^\circ \times 1^\circ$) between 4° W– 16° E and 39° – 51° N. Since in the Alps many terrain features are not well resolved by a $0.2^\circ \times 0.2^\circ$ resolution, a starting height for the released particles of 3000 m a.s.l. was used, which lies between the real elevation of the JFJ station (3580 m a.s.l.) and the model ground at ~ 2500 m a.s.l. Previous studies (Keller et al., 2011; Brunner et al., 2012) reported best model performance with this selection.

FLEXPART provided emission sensitivities (footprints) with a horizontal resolution of $0.1^\circ \times 0.1^\circ$, covering the Eu-

ropean region shown in Fig. 5). The surface footprints were then categorised according to the clustering technique detailed in Sturm et al. (2013) and Pandey Deolal et al. (2014). Here, seven categories were distinguished and can be identified by their main source region, i.e. the region with largest intensity of surface influence (see caption of Fig. 5).

2.5 Characterising air masses: influence of the planetary boundary layer

Although the JFJ's elevation above the surrounding low lands is well above typical PBL heights (see e.g. Seidel et al., 2010; Chan and Wood, 2013), frequent transport of polluted air masses from the PBL can be observed, as is the case for many mountainous sites (Rotach and Zardi, 2007). This transport is mainly driven by three processes (Zellweger et al., 2003; Forrer et al., 2000): dynamically by deflection of synoptic winds over mountainous terrains (e.g. Foehn winds), vertical turbulent mixing over flat terrain and advection to the JFJ (e.g. thunderstorms) or thermally by anabatic mountain winds. Especially during the warm season the thermal vertical transport drawing in PBL air from a radius up to ~ 80 km (Weissmann et al., 2005) leads to frequent increases of aerosol concentrations during the afternoon hours (Henne et al., 2005). This thermal transport results in the creation of a dynamically decoupled injection layer (IL) (Nyeki et al., 2000).

In the literature, several methods for the separation of FT air from IL air have been described. In the context of this study three methods were selected and applied: ^{222}Rn concentrations as tracer (Griffiths et al., 2014), the ratio of the sum of oxidised nitrogen species (NO_y) to carbon monoxide (CO), i.e. NO_y/CO as tracer (Zellweger et al., 2003; Pandey Deolal et al., 2013) and back trajectory analysis using footprint clustering (more details in Sect. 2.4). Figure S2 shows an example time series of both ^{222}Rn and NO_y/CO . Both methods assume different signatures in the FT and the IL. ^{222}Rn is naturally emitted from ice-free land surfaces (Yamazawa et al., 2005; Griffiths et al., 2014) and has a half-life of less than 4 days. Hence, elevated ^{222}Rn concentrations at the JFJ are a good indicator for influence of air masses with boundary layer origin. A threshold of 1.5 Bq m^{-3} was chosen with periods with ^{222}Rn concentrations below the threshold categorised as FT conditions. This choice of threshold is in accordance with the recommendations from Griffiths et al. (2014) ($0.75\text{--}2 \text{ Bq m}^{-3}$). The NO_y/CO ratio is a suitable proxy for the “age” of an air mass with ratios of 0.1 to 0.16 close to anthropogenic sources and ratios of < 0.01 after a few days of transport (Jaeglé et al., 1998; Stohl et al., 2002). Zellweger et al. (2003) reported NO_y/CO ratios of 0.002 to 0.005 for free tropospheric conditions at the JFJ, depending on the season. In this study, a threshold ratio of 0.004 was selected. Both thresholds are in accordance with the thresholds found by Herrmann et al. (2015) at the same site. A comparison of the ^{222}Rn and NO_y/CO time traces in Fig. S2 shows similar behaviour with radon being the

slightly stricter criterion – ²²²Rn: free tropospheric conditions during 41.1 % of the overlapping measurement period, NO_y / CO: free tropospheric conditions during 47.7 % of the overlapping measurement period. These fractions are higher than the annual fractions reported by Herrmann et al. (2015) (25.7 and 39.1 %, respectively), which is due to the inclusion of two summers (injection of PBL air is more frequent in summer) and a longer period without measurement in winter 2012/2013 (see Fig. 1a). In contrast, cluster no. 1 of the backward dispersion (BD) analysis identified as FT was only active during 11.2 % of the overlapping measurement period due to selection of BD only with maximal time (10 days) passed since last PBL contact (*t*_{PBL}). A more careful exploration of this parameter as it is performed by Herrmann et al. (2015) may allow for a lower *t*_{PBL} threshold.

2.6 Saharan dust events

Transport of dust plumes from the Saharan desert (SDE for Saharan dust event) up to the latitudes of the JFJ happens several times a year (Schwikowski et al., 1995; Collaud Coen et al., 2004; Bukowiecki et al., 2015). These plumes sometimes carry sufficient material with them that the dust can be seen by the naked eye as a brown-reddish layer on the Great Aletsch glacier and all other snow-covered surfaces. According to Collaud Coen et al. (2004), the distinctively different size, index of refraction and chemical composition of the SDE particles compared to the usual aerosol at the JFJ make SDEs easily detectable by their optical properties: while typically the exponent of the single scattering albedo (SSA) increases with wavelength, it decreases if mineral dust is present. The SSA is routinely measured by a nephelometer and an aethalometer at the JFJ. During the study period, eight extended SDEs (longer than 12 h) were detected. These periods are highlighted in light brown in Fig. 1b.

3 Results

3.1 Time series and concentrations

The top and middle panels of Fig. 1 show the full time series of organics (green), sulfate (red), nitrate (blue), and ammonium (orange) in the aerosol measured by the ToF-ACSM and the equivalent black carbon (black) concentration time series measured by the aethalometer from 27 July 2012 to 2 October 2013 in relative (top) and absolute (middle) terms. On top of Fig. 1b the periods used for the separation of seasons in the seasonal analyses of the following sections are identified. Saharan dust events are highlighted in light brown in the middle panel. In the summer periods average concentrations of all species were significantly enhanced compared to winter. The two bottom panels of Fig. 1 show expanded views of typical periods during summer (left) and winter (right). In summer the concentrations exhibit a strong variability between night/morning and afternoon/evening. While

total PM₁ concentrations in the night and morning usually were below 1 µg m⁻³, they increased to several µg m⁻³ in the evening hours (maximum 9.6 µg m⁻³ on 1 August 2012, 20:50 UTC). This pattern is caused mainly by thermally induced vertical transport and injection of PBL air up to the altitudes of the JFJ as detailed in Sect. 3.1.3. Usually concentrations decrease again during the night. Night-time elevated levels, e.g. 12 to 13 August 2012 (Fig. 1c, left), were caused by larger-scale meteorology. In the example above, a likely reason is a thunderstorm (several instances of remote lightning detected in the evening of the 12th) causing large-scale turbulences, i.e. vertical mixing of air masses which then were subsequently transported to the JFJ site. Additionally, several short-term spike-like increases in the organic fraction can be observed during daytime (also before the vertical mixing sets in). These spikes are attributed to local pollution by tourism or construction-related activities (cf. Sect. 3.2.1). It is noted that the resolution of Fig. 1b which shows the whole 14-month measurement period does not allow discrimination of spikes, and therefore average concentrations given in Fig. 2 cannot be estimated by eye from Fig. 1b. There are no afternoon increases in winter and concentrations are typically below 0.3 µg m⁻³ (less than during night and morning in summer). The daytime spikes are likewise visible, however smaller than in summer due to decreased tourism activity in the cold season.

3.1.1 Seasonal variations

In Fig. 2 the statistics for each season of the species mass concentrations, measured by the ACSM are shown in absolute and relative terms (including eBC). Corresponding concentration values for each species and season are given in Table 1. It is evident that the mean concentrations in every case lie well above the median concentrations due to the strong increases during injection of air masses from the PBL, which results in a skewed distribution of the observations (note the logarithmic scale of the y axes). Generally SO₄²⁻ and organics were the dominant species, together comprising 73 to 81 % of the total PM₁ mass over all seasons. NO₃⁻, NH₄⁺ and eBC contributed lower amounts, with none of these species accounting for more than 10 % of the mass in any season. Average contributions as well as absolute mass concentrations agree well with previous short-term AMS studies which reported average NR-PM₁ concentrations of 1.7 µg m⁻³ in March 2004, 2.5 µg m⁻³ in July/August 2005 (Cozic et al., 2008) and 1.6 µg m⁻³ in May 2008 (Lanz et al., 2010). A winter period from February/March 2005 reported in Cozic et al. (2008), which had atypical, spring-like meteorological conditions, featured much higher absolute concentrations (2.5 µg m⁻³) than recorded during winter in the present work (0.4 µg m⁻³).

Organic species dominated the total PM₁ mass, especially during the warm months (summer 2012 and 2013) when transport from the PBL was most abundant. In summer, the

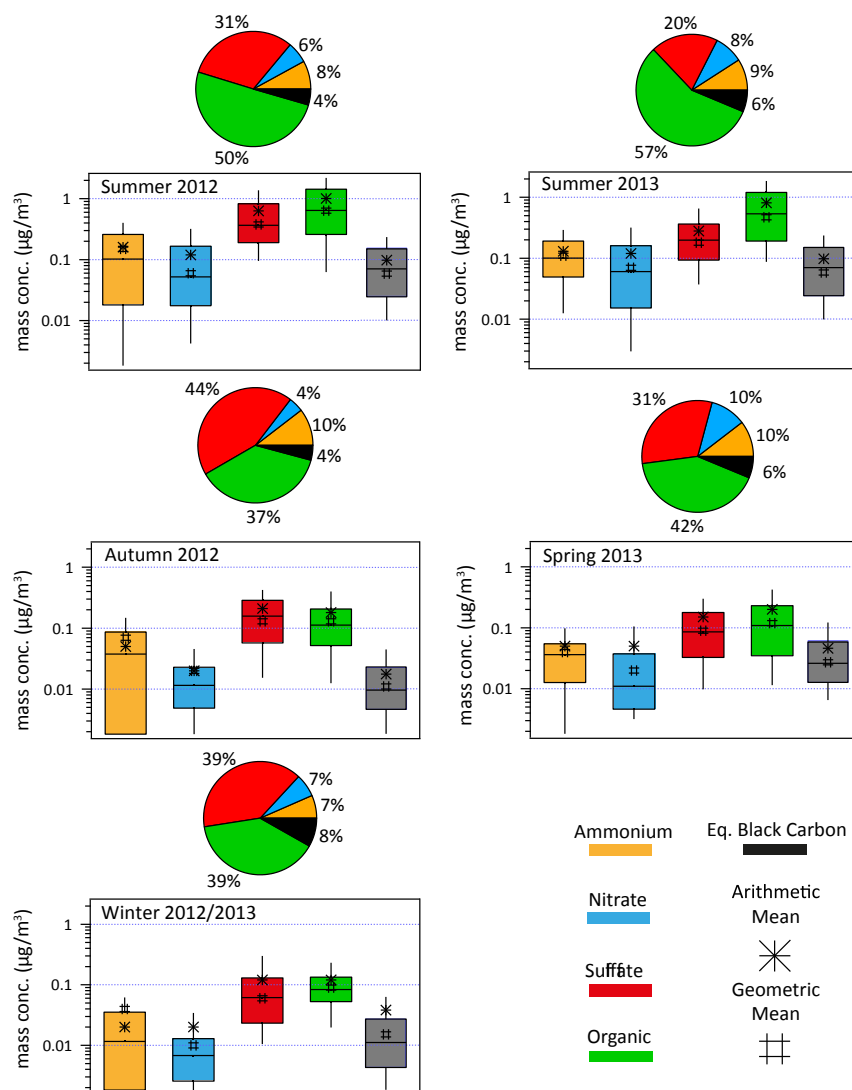


Figure 2. Pie charts of the relative average concentration and boxplots (in $\mu\text{g}/\text{m}^3$; line: median; box: interquartile range; whiskers: 10–90th percentile range) separated by seasons (summer 2012, autumn 2012, winter 2012/2013, spring 2013 and summer 2013) for species measured with the ACSM (organic: green; sulfate: red; nitrate: blue; and ammonium: orange) and eBC derived from optical absorption measurements. The arithmetic mean of each species is indicated by a star and the geometric mean by a hash in the respective boxplot. Mean and median concentration values for each species and season can be found in Table 1. Relative concentrations are given in percent in the pie charts.

contribution of organics to total PM₁ was between 50 and 57 %, while during the rest of the year it remained between 37 and 42 %. Average absolute concentrations of organics were around $1 \mu\text{g}/\text{m}^3$ during summer. In autumn, winter and spring they only amounted to 0.18, 0.16 and $0.20 \mu\text{g}/\text{m}^3$, respectively. This seasonal pattern of organic mass concentrations indicates that the organics in the FT mainly originate from organics that are emitted or formed in the PBL and mixed into the FT, while SOA production within the FT gives a minor contribution.

Sulfate was the dominant PM₁ species in autumn (44 %), while in winter sulfate and organics were equally abundant

(39 %). Absolute concentrations of sulfate did not vary as much between winter and summer as other species. This can be explained as follows: the atmospheric lifetime of SO₂ is, due to the low oxidation rate, similar to or longer than the timescale for mixing of PBL air into the FT air (Lee et al., 2011). This results in moderate vertical gradients of SO₂ and thus formation of sulfate within the FT. Consequently, the difference between the sulfate concentration in the PBL and the FT is moderate (cf. Sect. 3.1.3), and the seasonal pattern of the sulfate concentration in the FT is weaker than that of particulate species, which are exclusively emitted/formed in the PBL.

The nitrate-to-sulfate ratio observed in this study at the JFJ is low, in accordance with previous results from the JFJ (Henning et al., 2003; Herich et al., 2008) and other high-elevation sites around the world (e.g. Hidden Valley, Nepal, 5050 m a.s.l., Shrestha et al., 1997; Vallot Observatory, France, 4361 m a.s.l., Preunkert et al., 2002; Mauna Loa, USA, 3397 m a.s.l., Galasyn et al., 1987). This can be explained with the faster production of nitrate from NO_x compared to sulfate from SO₂. Therefore, NO_x is rapidly depleted with increasing age of air masses such that most nitrate formation occurs within the PBL, whereas nitrate formation within the FT is of minor importance. Accordingly, the ratio between nitrate concentration in the PBL and nitrate concentration in the FT is larger than the ratio for sulfate (cf. Sect. 3.1.3), and nitrate at the JFJ shows a distinct seasonal pattern linked to vertical transport.

Indeed, nitrate was generally low (highest average concentrations of 0.12 µg m⁻³ in the summers of 2012 and 2013), with exceptionally low median values in autumn and winter when transport from the PBL was less frequent. However, the large 90th percentile and a closer look at the full time trace of nitrate in Fig. 1b in winter reveal occasional strong increases of NO₃⁻ possibly attributed to special synoptic conditions that favour orographically driven vertical transport that can also occur in the colder seasons.

The ammonium mass fraction approximately corresponds to the amount required to neutralise the inorganic cations (sulfate and nitrate). Accordingly, the ammonium shows a small seasonal variability (7–10 % mass fraction) as the inorganic mass fraction varies between 28 and 48 % mass fraction. It is important to note that neutralised aerosol does not imply excess ammonia, as nitric acid only partitions into the particle phase in significant amounts together with ammonia. Therefore, the amount of particulate phase ammonium nitrate may be limited by the availability of either gas-phase ammonia or gas-phase nitric acid. Furthermore, it is noted that recent studies have shown that the molecular ratio, i.e. degree of neutralisation, is not a good proxy for the determination of aerosol pH aside from giving very rough information on whether an aerosol is alkaline or acidic (Hennigan et al., 2015; Guo et al., 2015).

Equivalent black carbon concentrations were between 4 and 6 % year-round except in winter (8 %). During winter the concentrations were lower in general, leading to an increased influence on the total mass of occasional PBL contributions. The correlation of the eBC concentrations with the overall yearly cycle (i.e. higher total PM₁ concentrations with higher outside temperatures; see Fig. S3) presumably is mostly related to increased vertical pollution transport, which is implied by good covariance with nitrate mass. The higher eBC fraction in summer 2013 compared to summer 2012 may in parts be related to increased local construction work activity in 2013 including the operation of diesel engine generators, but also to higher organic concentrations in 2012.

In summary, the seasonal variations of concentration and chemical contribution showed the importance of the injection layer and hence aerosol transport from the PBL in the vicinity of the JFJ for the total measured concentrations at the JFJ.

3.1.2 Diurnal variations

Median and mean diurnal cycles (in µg m⁻³) of organic, ammonium, nitrate, and sulfate for each season are shown in Fig. 3. Thermally induced transport caused increased nitrate and to a lesser extent also organic mass concentrations in the afternoon starting around 11:00 to 12:00 UTC and peaking between 16:00 and 18:00 UTC. This behaviour was strongest during the summer periods (orange: 2012; red: 2013) and also evident in spring (green), but mostly absent in autumn (brown) and winter (blue).

The diurnal pattern shows that injections from the PBL result in substantially increased nitrate and organic particulate mass concentrations. This can be attributed to the fact that they are mainly emitted and formed within the PBL, as already argued in Sect. 3.1.1. In contrast, sulfate only exhibits a very weak diurnal pattern. This indicates that the sulfate concentrations in the upper PBL are similar to those in the FT, as it is also produced in the FT (cf. Sect. 3.1.1). The relative magnitude of the diurnal cycle of ammonium lies in between those of nitrate and sulfate.

Generally, the concentrations observed during summer 2012 and 2013 were comparable for all species except SO₄²⁻. A partitioning of both summers by air mass origin showed an increased frequency of southerly origins (51 % in summer 2012 vs. 39 % in summer 2013; cf. Fig. S4) at the expense of air mass transport from the north. In Sect. 3.1.4 it is shown that air masses arriving from the south on average were carrying more sulfate, which leads to higher SO₄²⁻ concentrations in summer 2012. Mean and median show the same trends except in autumn 2012 where the mean diurnal cycles of organics and nitrate showed a strong increase during daytime, while no such increase is seen in the median. This increase stems only from 1 day (14 October 2012) when especially high nitrate concentrations (the highest values of the whole campaign, up to 4 µg m⁻³) and increased concentrations of all other species were measured. This was attributed to non-thermally induced transport of air masses from the valley floor (frontal lifting). Mean concentrations of NH₄⁺ and SO₄²⁻ were not or only little affected because elevated concentrations of both are measured more frequently in autumn 2012, while NO₃⁻ is close to zero during most of autumn 2012.

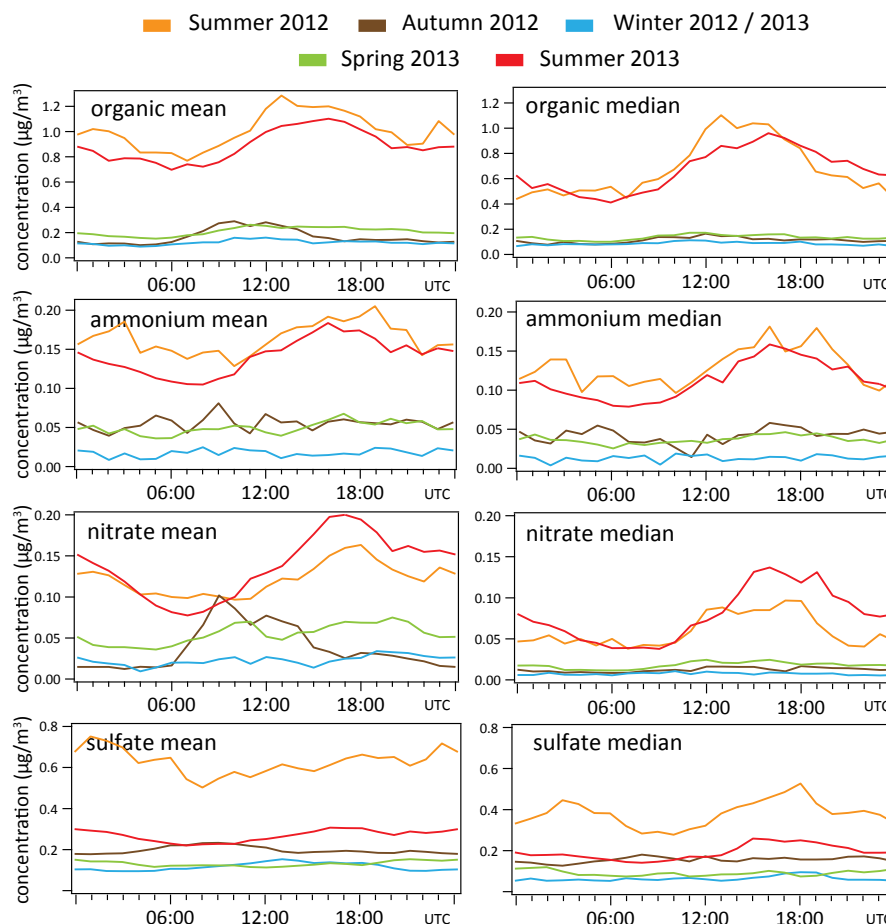


Figure 3. Seasonal diurnal plots for organics, ammonium, nitrate and sulfate (from top to bottom) in $\mu\text{g m}^{-3}$. On the left: mean diurnal concentrations; on the right: median diurnal concentrations. The different traces show the seasons: summer 2012 in orange, autumn 2012 in brown, winter 2012/2013 in blue, spring 2013 in green and summer 2013 in red. Times are shown in UTC.

3.1.3 Free tropospheric concentrations

Three methods to distinguish periods with free tropospheric air masses at the JFJ from periods with recent influence of the PBL were compared, using the ToF-ACSM data set to explore the chemical composition of FT air. Figure 4a shows the median concentrations during periods independently classified as free tropospheric conditions by the three criteria introduced in Sect. 2.5: ^{222}Rn , NO_y/CO and BD clustering. All three methods yielded similar median concentrations comparable to the mean concentrations in winter: $0.10\text{--}0.12\text{ }\mu\text{g m}^{-3}$ of organics, $0.02\text{--}0.03\text{ }\mu\text{g m}^{-3}$ of NH_4^+ , $0.16\text{--}0.18\text{ }\mu\text{g m}^{-3}$ of SO_4^{2-} , $0.01\text{ }\mu\text{g m}^{-3}$ of NO_3^- and $0.02\text{ }\mu\text{g m}^{-3}$ of eBC.

The boxplots of Fig. 4b–d show both, concentrations during FT conditions (left boxes, highlighted in light blue) and times when PBL aerosol reached the JFJ (non-FT, right boxes, highlighted in light yellow) with mean (star) and median (horizontal line) indicated in the plots and given as numbers above each boxplot. The boxes indicate the interquartile

range (IQR) and the whiskers the 10th and 90th percentiles. Again, a comparison of (b), (c) and (d) shows good agreement of all three methods with slightly lower FT concentrations for the BD method. This difference may arise from a more strict FT definition used by the BD method: only BD without significant PBL contact during the last 10 days was assigned to the FT cluster. Each method uses specific cut-off parameters, i.e. FT thresholds which are all subject to uncertainties. A more strict cut-off will lead to lower mean concentrations during both FT and non-FT conditions.

A comparison of the median concentration values (^{222}Rn or NO_y/CO criterion) during non-FT and FT conditions yielded ratios of 1.8 for organics and 1.7 for NH_4^+ , a higher ratio of 2 to 3 for NO_3^- and a lower ratio close to 1 : 1 for SO_4^{2-} . This is consistent with the interpretation of the diurnal patterns (Sect. 3.1.2) suggesting that the aerosol from PBL injections has higher mass concentrations and mass fractions of organics and nitrate compared to the FT aerosol. A more detailed look at the mass spectra (local primary or-

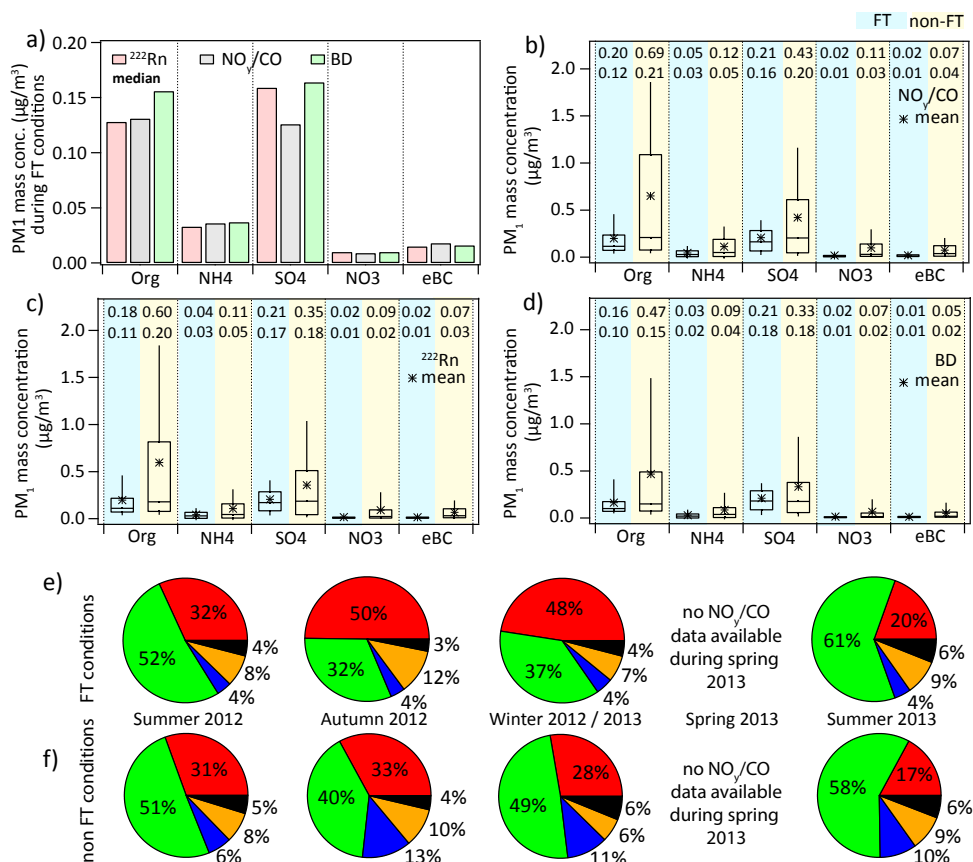


Figure 4. (a) Median NR-PM₁ species concentrations during free tropospheric conditions for three different criteria of FT separation: ²²²Rn, NO_y / CO and backward dispersion clustering. (b, d) Show mean (star) and median (horizontal bar) concentrations for each species measured by the ToF-ACSM during the periods with data for all three different criteria – (b): NO_y / CO, (c) ²²²Rn, (d) BD clustering. Blue background: FT condition; yellow background: non-FT condition. Absolute mean (top) and median (bottom) values in µg m⁻³ are given above each plot. The boxes represent the IQR and the whiskers the 10th to 90th percentile range. The pie charts show the relative species concentration of SO₄²⁻ (red), NH₄⁺ (orange), NO₃⁻ (blue) and organics (green) for FT conditions (e) and for non-FT conditions (f) separated by seasons using NO_y / CO for FT discrimination. No NO_y / CO ratios were available in spring 2013. ²²²Rn data were not available after February 2013.

ganic aerosol contributions were subtracted from the spectra in advance; cf. Sect. 3.2.1) showed a non-FT / FT ratio of the signal at m/z 44 of 1.9, which is comparable to the non-FT / FT ratio for total organic mass. However, m/z 55, 57 and 60, which are mainly related to primary sources, showed larger ratios of around 3 (m/z 55: 2.9; m/z 57: 3.6; m/z 60: 3.3) similar to NO₃⁻. These values are similar to m/z 43 (3.0), which is present in primary OA but also in less oxidised SOA. These results indicate an increased importance of primary OA (POA) sources during periods when PBL aerosol was injected into the JFJ region.

Similar conclusions could be drawn from the differences of the (seasonal) relative species fractions between FT (Fig. 4e) and non-FT conditions (Fig. 4f). During autumn and winter the fraction of SO₄²⁻ was increased by about 60 % during FT conditions, while the organic fraction was decreased by about 30 %. The NO₃⁻ fraction showed by far the largest

difference with a decrease of about a factor 3 during FT conditions (autumn and winter). The NH₄⁺ contributions, however, stayed more or less the same. The difference between FT and non-FT conditions was much smaller in both summers, also showing decreased NO₃⁻ during FT conditions but largely similar contributions of the other species. These observations lead to several conclusions: (1) most nitrate measured at the JFJ was injected from the PBL, (2) significant amounts of organics were injected from the PBL, (3) sulfate loadings in the FT and upper PBL are similar such that PBL influence does not cause distinct diurnal or seasonal patterns, (4) the constant NH₄⁺ fraction through all seasons is due to the compensating effects of NO₃⁻ and SO₄²⁻ with which NH₄⁺ is associated, and (5) in summer aerosol levels remained elevated and retained a similar chemical composition also during FT conditions, indicating an overall larger PBL influence on the regional-scale lower free troposphere.

Long-term ACSM measurements at a site in the Magadino plain (Switzerland, 204 m a.s.l., latitude: 46°9′37″ N, longitude: 8°56′2″ E) showed comparable species contributions in summer 2014 (see Fig. S5). Similar findings of decreased nitrate and enhanced sulfate and organic concentrations during FT conditions were reported from the French elevated site Puy-de-Dôme (1465 m a.s.l.) by Freney et al. (2011).

3.1.4 Geographical aerosol origins

Its central European location makes the JFJ a good receptor site for pollutants from different source regions within Europe (and beyond, e.g. SDE). A clustering of air mass origin into seven footprint regions is shown in Fig. 5 together with the corresponding NR-PM₁ aerosol composition and equivalent black carbon. Mean and median concentrations of each cluster are given below the pie charts. For all clusters good statistics with total measuring times between 765 h and 1527 h were achieved. The clusters are numbered from no. 1 to no. 7 and can be characterised by the prevailing cardinal directions/origins (cf. Table 2, including frequencies of each cluster.)

It should be noted again that footprints were calculated using meteorological input data with a horizontal resolution of $0.2^\circ \times 0.2^\circ$. While these simulations are able to capture the large-scale synoptic flow, local meso-scale flow patterns in the complex mountain topography are not represented well in the model and are only estimated by the inclusion of enhanced turbulent transport over terrain with large sub-grid-scale topography variations (Stohl et al., 2005). Hence, some locally driven transport events may be missed by the model and could be misclassified by the BD clustering.

Highest mean and median total concentrations were recorded from clusters no. 3 to no. 5 (south-west to south-east directions) with average concentrations between 1.59 and $1.63 \mu\text{g m}^{-3}$ (median: 0.63 – $1.03 \mu\text{g m}^{-3}$). Clusters no. 6 and no. 7 (north-west to north-east directions) showed about 20 % lower mean concentrations between 1.25 and $1.37 \mu\text{g m}^{-3}$ (median: 0.55 – $0.69 \mu\text{g m}^{-3}$) and cluster no. 2 (west) showed ~ 50 % lower mean concentrations of $0.85 \mu\text{g m}^{-3}$ (median: $0.43 \mu\text{g m}^{-3}$). The free tropospheric cluster no. 1 showed an equally low median ($0.40 \mu\text{g m}^{-3}$) but higher mean, indicating a stronger influence of regional transport phenomena that was not captured by the transport model. A possible explanation is a frequent connection between subsidence (i.e. FT air masses) and anticyclonic conditions leading to fair weather with higher temperatures (i.e. increased thermally induced regional vertical transport).

A comparison of the different aerosol chemical species showed dominant organic aerosol from all regions, with highest OA concentrations from the north-west (63 %) and for the FT cluster (66 %) and lowest OA concentrations from the south (43 %). Sulfate was most abundant in air masses from the southern (no. 3: 27 %; no. 4: 33 %; no. 5: 27 %) and western regions (no. 2: 28 %). The lowest sulfate frac-

tion was detected from the north-west (17 %). Nitrate fractions were relatively constant (8–10 %) from all regions with slightly lower contributions in clusters no. 1 and no. 2 (6 %). The same was true for eBC which ranged between 3 and 5 %. Large fractions of the total NO_3^- and eBC are expected to be imported from the regional boundary layer (cf. Sect. 3.1.3). The level of ammonium depended on the sum of NO_3^- and SO_4^{2-} , suggesting mainly ammonium nitrate and ammonium sulfate aerosol in all clusters.

Summarised, PM₁ concentrations in air masses advected from south of the Alps (where regions with known high aerosol loadings like the Po Valley are located; cf. van Donkelaar et al., 2010) were about 20 % higher (BeNeLux, UK, Germany) to 50 % higher (France, Atlantic) than the PM₁ in air masses from north of the Alps (Germany, Scandinavia). These air masses also carried higher fractions of sulfate aerosol, while in the northern air masses larger fractions of organic aerosol were measured. This higher sulfate mass fraction was also observed if only FT air masses in clusters no. 2 to no. 7 using the NO_y/CO criterion for additional air mass separation were considered. 45 % of the mass was sulfate in FT air masses from clusters no. 3, no. 4 and no. 5, while the mass fraction of sulfate from the northern clusters no. 6 and no. 7 is at 29 % (cf. pie charts in Fig. 6). The apparent discrepancy between organics dominance in cluster no. 1 and the above analysis where, for FT conditions, sulfate was most abundant, is due to the fact that the footprint analysis is mostly restricted to northern air masses in cluster no. 1, while sulfate is higher with southern air masses. Air masses advected from the west over France and the Atlantic Ocean carried the lowest mean aerosol loading but a sulfate fraction comparable to aerosols from the south. This could be a hint towards influence of shipping emissions off the Atlantic coast.

3.2 Organic mass spectra

A large fraction of all m/z channels in the aerosol mass spectra is attributed to organic compounds. However, fragmentation, thermal decomposition and partly also insufficient mass resolution (although the possibility of limited high-resolution peak fitting of ToF-ACSM data has been demonstrated by Fröhlich et al., 2013) cause the loss of information about the parent compounds. Nevertheless, techniques like ME-2 or PMF allow for a further separation according to emission/production sources. Furthermore, a closer look at m/z channels known to be dominated by well-understood ions can shed more light on the evolution and sources of the organic fraction.

Figures 7a–e show the fractions of total OA (the contributions of a minor local primary OA factor – see Sect. 3.2.1 – were subtracted for total OA beforehand) of the UMR m/z 43, 44, 55, 57 and 60 (f_{43} , f_{44} , f_{55} , f_{57} and f_{60}). A clear maximum during the summer periods and the minimum in winter of f_{43} can be recognised, while f_{44} stayed more or

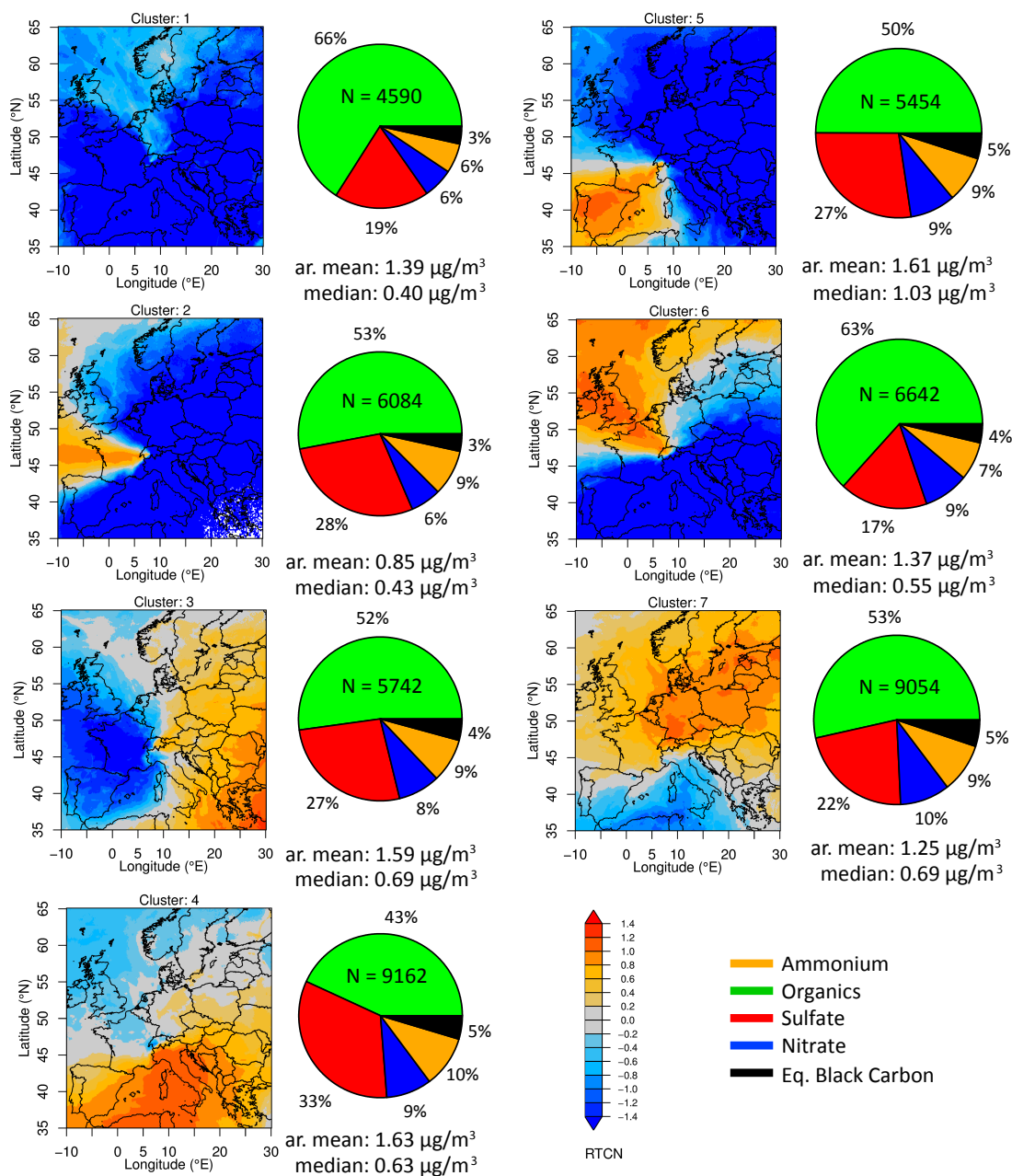


Figure 5. Aerosol footprint clusters with corresponding relative contributions of PM₁ organics (green), sulfate (red), nitrate (blue), ammonium (orange) and equivalent black carbon (black). Arithmetic mean as well as median total concentrations are given below each pie chart. The number N in each pie chart indicates the number of 10 min averages included in the calculation of the mean and median. The unitless RCTN (residence times by cluster normalised) shows the normalised difference between cluster average and total average residence times. Positive (negative) values indicate increased (decreased) surface sensitivity compared to the overall footprint. The scale extends from -2 to 2 with values larger than 1 (smaller than -1), indicating regions with at least 3 times longer (shorter) residence times; for details, see Sturm et al. (2013).

less constant throughout the year. Both of those m/z are typically found in secondary organic aerosols (SOA), with f_{43} being more abundant in more recently formed SOA (Chhabra et al., 2010; Pfaffenberger et al., 2013), while f_{44} increases with age and oxidation state (Ng et al., 2010, 2011a). Addi-

tionally, f_{43} is an important fragment in many POAs (e.g. cooking, traffic). A constant f_{44} points towards similarly aged background aerosols in summer and winter and the increase of f_{43} during the summer is attributed to vertical transport of: (1) less oxidised SOA (possibly associated with

Table 1. Mean and median concentrations in $\mu\text{g m}^{-3}$ during each season.

Geometric mean	Summer 2012	Autumn 2012	Winter 2012/13	Spring 2013	Summer 2013	Annual mean*
Organic	0.64	0.13	0.09	0.12	0.47	0.13
Sulfate	0.38	0.13	0.06	0.09	0.18	0.09
Nitrate	0.06	0.02	0.01	0.02	0.07	0.02
Ammonium	0.16	0.07	0.04	0.04	0.11	0.05
eBC	0.05	0.01	0.02	0.03	0.06	0.02
Sum NR-PM ₁ and eBC	1.29	0.36	0.22	0.30	0.89	0.31
Arithmetic mean						
Organic	1.01	0.18	0.12	0.20	0.81	0.25
Sulfate	0.63	0.21	0.12	0.15	0.28	0.17
Nitrate	0.12	0.02	0.02	0.05	0.12	0.04
Ammonium	0.16	0.05	0.02	0.05	0.13	0.05
eBC	0.10	0.02	0.04	0.05	0.10	0.05
Sum NR-PM ₁ and eBC	2.02	0.48	0.32	0.50	1.35	0.55
Median						
Organic	0.64	0.11	0.08	0.11	0.54	
Sulfate	0.37	0.16	0.06	0.09	0.20	
Nitrate	0.05	0.01	0.01	0.01	0.06	
Ammonium	0.10	0.04	0.01	0.04	0.10	
eBC	0.07	0.01	0.01	0.03	0.07	
Sum NR-PM ₁ and eBC	1.23	0.33	0.17	0.28	0.97	

* Annual geometric/arithmetic mean weighted by seasonal data cover for the period 1 October 2012 to 1 October 2013.

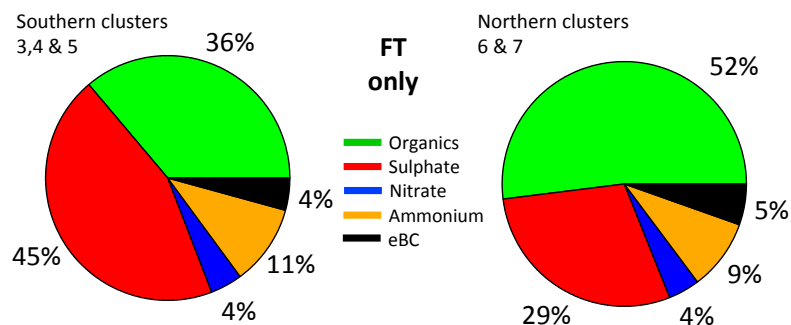


Figure 6. Relative species contributions only during FT conditions separated by air mass origin. Left: southern air masses (clusters no. 3, no. 4 and no. 5 of Fig. 5); right: northern air masses (clusters no. 6 and no. 7 of Fig. 5). Note that contributions of cluster no. 1 were not considered.

Table 2. Transport footprint clusters and main origins.

Cluster	Main origin in PBL	Frequency
No. 1	No recent PBL contact/free tropospheric	11.3 %
No. 2	West	14.9 %
No. 3	East/south-east	14.1 %
No. 4	South	22.5 %
No. 5	South-west	13.4 %
No. 6	North-west	16.3 %
No. 7	North/north-east	22.2 %

increased emission of biogenic SOA precursors by plants) and (2) f_{43} containing POA. An investigation of the POA and SOA factors found in the OA source apportionment of Sect. 3.2.1 showed POA contributions to f_{43} between 17.8 and 65.9 % depending on the season (summer 2012: 17.8 %, autumn 2012: 40.1 %, winter 2012/2013: 65.9 %, spring 2013: 35.7 %, summer 2013: 18.7 %).

The major part of f_{57} is usually attributed to hydrocarbon-like emissions e.g. by combustion engines (Zhang et al., 2005). No clear trend is visible for f_{57} . It contributed around 0.5 % year-round which suggests a generally low, but constant influence of HOA at the JFJ. Part of the OA fraction at

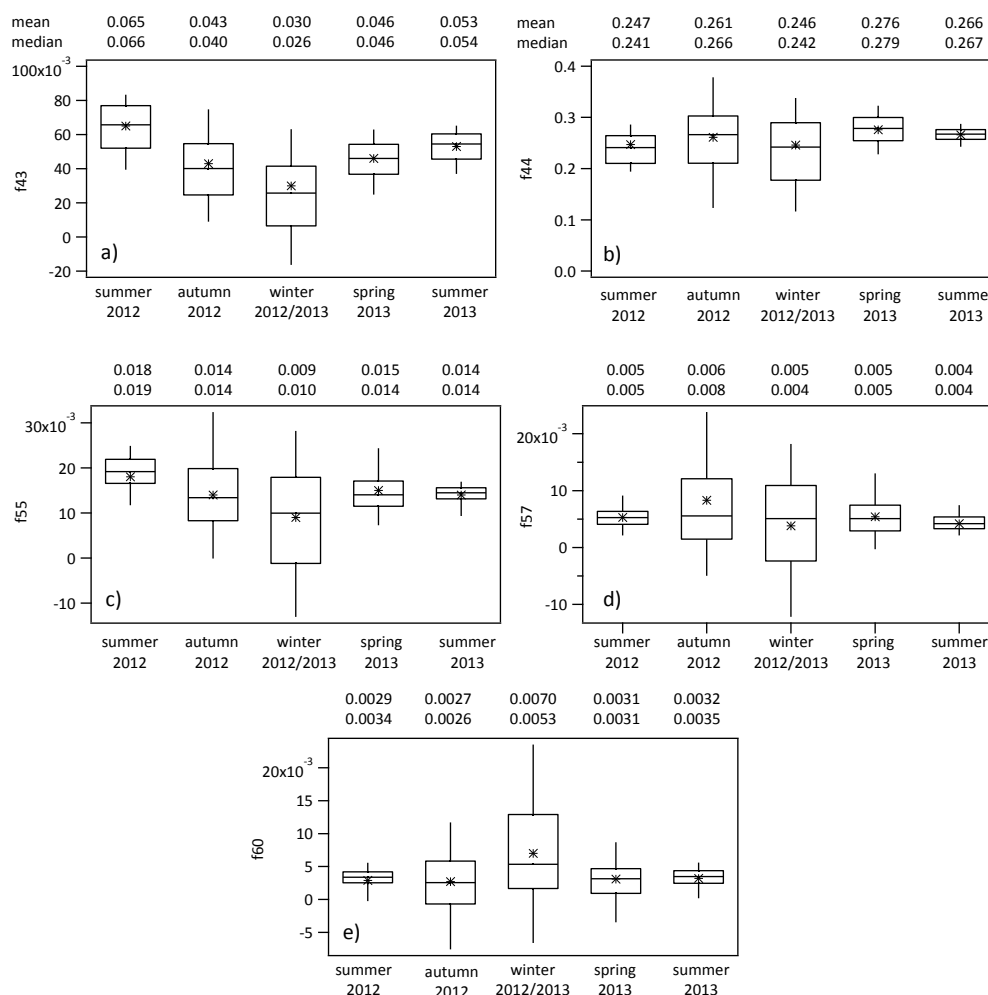


Figure 7. Seasonal variation of fractions of total OA for different mass-to-charge ratios: (a) f_{43} , (b) f_{44} , (c) f_{55} , (d) f_{60} . Mean (star) and median (horizontal bar) values are given above each boxplot. The IQR is shown as a box and the 10th to 90th percentile range as whiskers. The contribution of local primary organic aerosols was subtracted from the mass spectra before calculation of the fractions. It is noted, that the increased width of the distribution in winter and autumn is due to smaller signal-to-noise ratio during these seasons.

m/z 55 is also attributed to HOA emissions, but f_{55} also has other important sources like cooking (Mohr et al., 2012) or SOA at lower oxidation stages. The f_{55} followed the same trend as f_{43} and was elevated during the summer period, which was likewise due to increased up-slope transport. The effect of varying local pollution was accounted for by subtracting the local POA identified by ME-2 from the organic mass spectra (for details see Sect. 3.2.1). The winter/summer difference was a little more pronounced for f_{43} but overall the seasonal behaviour of f_{55} was comparable. The mean and median fraction of m/z 60 exceeded the 0.3 % threshold reported to be characteristic of biomass burning only in winter (Cubison et al., 2011).

The IQR of all fractions was increased during the colder months, which is mainly due to the increased influence of noise resulting from low concentrations. In general the anal-

ysis of these markers supported the conclusion of increased vertical transport from the PBL during summer and indicated biomass burning influence in winter, which could be either from longer-range transport or local (or regional) vertical mixing.

3.2.1 ME-2 results

ME-2 organic source apportionment was performed separately for all seasons to account for seasonal changes in factor profiles, especially OOA. Seasonal PMF for long-term data sets was also performed before by Minguillón et al. (2015) and Tiitta et al. (2014). Parworth et al. (2015) went one step further and were performing separate PMF analyses on shifting 2-week windows (which they call the “rolling window technique”) over a full period of 19 months to capture changes in the OOA and BBOA factors.

ME-2 input matrices with an m/z range of 12–120 were prepared. Higher m/z channels were omitted due to low signal to noise at the low mean concentrations prevalent at the JFJ. Errors were calculated accounting for Poisson counting statistics and electronic noise in accordance with Allan et al. (2003). Peaks calculated from m/z 44 were considered in the ME-2 analysis but their uncertainties were adjusted according to the recommendations of Ulbrich et al. (2009) to avoid overweighting.

The daily vertical mixing (during appropriate seasons) poses a challenge to the ME-2 analysis since PMF relies on unique source variabilities for a good separation of sources. Simultaneous advection of aerosols from different sources hence cannot be separated autonomously. The approach applied to deal with this issue can be described as an extended chemical mass balance (CMB, Watson et al., 1997; Ng et al., 2011b). A priori information of organic aerosol source spectra is introduced into the model using the a value technique available in ME-2. In the absence of distinct criteria for the determination of ideal a values due to contemporaneous advection of typical tracers a large range of a values was taken into account for the final result which ultimately constitutes the arithmetic mean of all reasonable solutions using the range of a values indicated in Table S1 in the Supplement. This table also contains reasons for the respective choice of a ranges. Variability (1σ) of the result as percent of the total source contribution is given in Table S2. There, in addition to the variability due to different a values, also the variability due to different random starting points of the ME-2 (seeds) is taken into account by averaging five seeds for each set of a values. It is noted that although large a value ranges were considered the variability usually is below $\pm 10\%$.

Three to five factors could be identified depending on season. During all seasons, a primary hydrocarbon-like OA (HOA), a locally emitted primary OA (POA_{loc}) and secondary oxygenated OA (OOA), which in summer was split up into LV-OOA I and LV-OOA II, could be identified. Due to the absence of direct volatility measurements the attribution of the OOAs to the LV-OOA family was made indirectly on the basis of spectral similarities to the range shown in Ng et al. (2010). A biomass-burning-related OA (BBOA) was identified when the signal of its most specific fragment peak at m/z 60 was above the background level. This occurred in winter as well as in summer 2013, when three distinct biomass-burning events were identified (presumably due to forestry-related fires; see Fig. S6). Mean HOA and BBOA reference spectra taken from Ng et al. (2011b) were used in the ME-2. The anchor spectrum of POA_{loc} was extracted directly from the data set by a separate unconstrained PMF only on all short-term peaks visible in the organic time series (cf. Fig. 1c). This separate PMF resolved (next to the always present background OOA) only one local primary OA factor, suggesting that the local emissions mainly came from a single local source. Also an additional k -means clustering analysis of all mass spectra of the short-term peaks (with sub-

traction of the background by interpolation of the spectrum before and after each peak) only resulted in a single cluster.

In the following analysis POA_{loc} always remained tightly constrained ($a = 0.05$), while for HOA (and if applicable, BBOA) many solutions with different a values (varied in steps of $\Delta a = 0.1$) were averaged. The OOAs were always completely unconstrained (no a priori mass spectrum).

As an example, the solution (time series and profiles) from summer 2012 is shown in Fig. 8a–c. All other solutions discussed here behave similarly and their time series and profiles can be found in the Supplement (Figs. S6 and S7). The profiles of Fig. 8a show a similarity between HOA and POA_{loc}, while the time series of these two factors are completely independent. HOA follows the general diurnal pattern influenced by vertical transport, similar to eBC (cf. Fig. S10) and POA_{loc} mainly consists of sharp short-term peaks only appearing during daytime (see zoom in Fig. 8c). It is noted that due to the large similarity of HOA and cooking-related (COA) profiles it cannot be excluded that a fraction of the presented HOA may be influenced by COA.

The two OOAs generally followed the same diurnal pattern as HOA with LV-OOA I showing less temporal variability and a higher relative signal at m/z 44 than LV-OOA II. This points towards a more aged oxidised OA. Although LV-OOA I presumably does have the lower volatility since it is more oxidised, the separation in this case was rather driven by origin or formation processes than by volatility since temperatures are always low at the JFJ. The vertical transport pattern was pronounced in the less oxidised LV-OOA II and it showed the same diurnal trends as nitrate (cf. Fig. S8), while the other (LV-OOA I) represents the background OOA and correlated better with sulfate (cf. Fig. S8). This indicates that further oxidation of the OA takes place in the FT.

The seasonal diurnal cycles of HOA, POA_{loc} and OOA are shown in the bottom panels of Fig. 8. HOA in (d) and LV-OOA II in (f) showed afternoon increases which were less pronounced in winter and autumn. LV-OOA I however exhibited a much less pronounced diurnal trend than LV-OOA II confirming its background nature. POA_{loc} (Fig. 8e) was mainly observed between 09:00 and 15:00 LT coinciding with the opening hours of the tourist facilities and the train to the JFJ. In autumn to spring, the concentrations of POA_{loc} outside the opening hours went down almost to zero, while in the peak tourist season in summer low concentrations of POA_{loc} were also found in the non-spiky background during the night, which indicates an imperfect separation of POA_{loc}, i.e. a small overestimation during the summers. The autumn diurnals were dominated by two large non-thermally induced vertical transport events on 14 and 26 October causing the peak between 06:00 and 14:00 UTC in HOA and OOA (see Figs. S6 and S7), similar to Sect. 3.1.2.

Relative source contributions for all five seasons between summer 2012 and summer 2013 are depicted in Fig. 9 as pie charts. Secondary OOA dominated the OA all over the year,

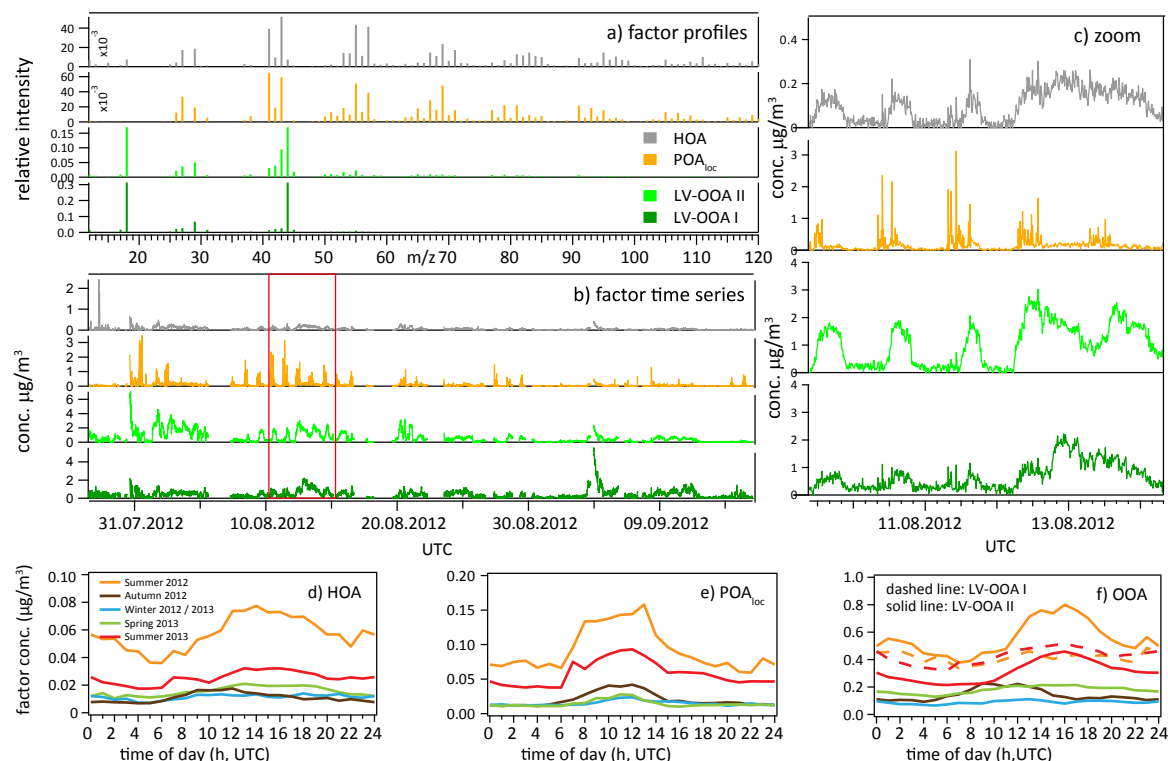


Figure 8. ME-2 example solution for summer 2012 and diurnal plots. **(a)** Factor profiles of HOA (grey), POA_{loc} (orange), LV-OOA I (dark green) and LV-OOA II (light green). **(b)** Factor time series of HOA, POA_{loc}, LV-OOA II and LV-OOA I. **(c)** Zoom of the region indicated in red (about 5 days) in the time series plot. **(d)** HOA diurnal cycles for all seasons. Orange: summer 2012; brown: autumn 2012; blue: winter 2012/2013; green: spring 2013; red: summer 2013. **(e)** POA_{loc} diurnal cycles for all seasons. **(f)** OOA diurnal cycles for all seasons. Dashed line: LV-OOA I; solid line: LV-OOA II. All times are in UTC.

constituting between 71 % (winter 2012/2013) and 88 % (summer 2013).

POA_{loc} contributed 7–8 % in both summers and spring and 12 % in autumn and winter. This means that relative contributions of POA_{loc} were higher in winter when non-local OA was generally low, while the absolute concentrations of POA_{loc} were higher in summer when there were more visitors at the station, i.e. a higher tourist activity. The time series of POA_{loc} overlaid with a shaded background in either blue (days when global radiation is below average) or red (days when global radiation is above average) is shown in the top panel of Fig. S9 for a period of 2 months in summer 2013. The bottom panel shows number concentrations measured with a CPC (time resolution 10 s) for the same period. A strong evidence for a connection of POA_{loc} to tourist activities is the generally lower occurrence of spikes during the (less sunny) “blue” days than the “red” days. This was confirmed by the CPC number concentrations, which also showed fewer spikes on the same days.

Possible sources of local pollution by tourism-related activities are cigarette smoke, fuel combustion by helicopters or snowcats, and emissions of the three on-site restaurants. Previous studies have shown that significant differences be-

tween source profiles of these three sources exist (see e.g. Mohr et al., 2009; Faber et al., 2013). The results of PMF and the cluster analysis on the spikes described above suggested a single source for the majority of the peaks. Figure S10 shows a one-week time series (7 to 13 August 2012) of HOA, POA_{loc}, eBC and CPC with high time resolution (for values cf. legend). The fact that eBC did not show any short-term spikes at all while POA_{loc} and CPC number showed many spikes during daytime allowed for the exclusion of combustion engines as likely POA_{loc} source, since they are expected to emit significant amounts of black carbon as opposed to cigarettes or restaurants (Hildemann et al., 1991; Kleeman et al., 1999). Furthermore, the spikes are too frequent (> 100), too regular and distributed over the whole day with time scales of one to a few minutes to have been emitted by occasional helicopter flybys (less frequent), irregular construction work (more constant emissions) or snowcat activities (typically only in the morning and evening). A correlation of the POA_{loc} profile (see Fig. S11) with known reference profiles of traffic and cooking (COA) resulted in R^2 of 0.74 for HOA from Ng et al. (2011b), $R^2 = 0.77$ for COA from Crippa et al. (2013) and $R^2 = 0.94$ for cigarette smoke OA from Faber et al. (2013). Only the m/z range be-

tween 45 and 120 was considered for the correlations to avoid uncertainties related to f_{44} (for details see Fröhlich et al., 2015). The cigarette smoke OA from Faber et al. (2013) is also shown in Fig. S11. The striking similarity of POA_{loc} and cigarette smoke OA above m/z 44 points towards smoking of cigarettes as the most likely source for the local pollution spikes. This assumption is supported by a concurrent increase in the near-ultraviolet (370 nm) absorption signal of the aethalometer (see Fig. S18). Tobacco smoke is known to have increased optical absorption at the near-ultraviolet wavelength compared to longer wavelengths (Hansen, 2005). Some of the f_{44} difference between POA_{loc} and cigarette smoke OA is expected due to the mentioned f_{44} uncertainties in the ACSM systems but the POA_{loc} exhibits a particularly low f_{44} close to zero. This may indicate that a small fraction of the POA_{loc} is misallocated to one of the other factors, most likely the OOA, partly offsetting the potential overestimation during night-time. In the literature, several cigarette smoke OA spectra were reported showing different amounts of f_{44} . The cigarette smoke OA of Northway et al. (2007) shows low f_{44} ($f_{44}/f_{43} \approx 0.08$), while Tang et al. (2012) show a f_{44}/f_{43} ratio of about 0.25 in sidestream environmental tobacco smoke and $f_{44}/f_{43} \approx 0.5$ in mainstream smoke, similar to Faber et al. (2013). However, ME-2 including a cigarette smoke OA anchor profile (or COA anchor profile) did not result in a similarly good separation of the local spikes from the HOA. It is noted that, also under the assumption that the “real” f_{44} was similar to Faber et al. (2013), the difference in the total POA_{loc} concentration was smaller than 10 %, which lies within the estimated uncertainties of the method reported by Fröhlich et al. (2015). Morrical and Zenobi (2002) have previously identified environmental tobacco smoke markers in the particulate phase at the JFJ in a non-quantitative way.

HOA contributions varied between 3 % (summer 2013) and 9 % (winter 2012/2013). The higher relative HOA fractions in the colder months can be explained by the large contribution to the total OA mass of a few vertical transport events containing higher amounts of HOA as opposed to the FT air masses (cf. HOA time series in Fig. S7). In addition, the restriction of the PMF output to positive values can cause a small positive bias at low concentrations. Absolute concentrations, however, were higher in summer due to increased overall influence of vertical transport. Previous PMF studies of a short-term AMS data set from May 2008 found HOA contributions of 6 % (Crippa et al., 2014) and 7 % (Lanz et al., 2010), similar to the 8 % found in this study for spring 2013.

Table 3 shows the HOA-to-BC ratios as a function of season. Values around 0.5 were observed, with the exception of summer 2013 when a significantly lower ratio of 0.27 was measured. A likely reason is a faster oxidation of the semi-volatile fraction of HOA reducing the remaining HOA/BC (Hildebrandt et al., 2010). Another possible influence on the changed ratio is increased construction work activity in

Table 3. Ratios of HOA to eBC for all seasons.

Season	HOA : BC
Summer 2012	0.56
Autumn 2012	0.54
Winter 2012/2013	0.43
Spring 2013	0.53
Summer 2013	0.27

summer 2013 (e.g. renovation of a restaurant roof) entailing the use of diesel engine generators possibly emitting higher amounts of eBC on site. A third possibility is an underestimation of HOA in the source apportionment during summer 2013. The reported ratios are in agreement with measurements in a Swiss highway tunnel (Gubrist tunnel) by Chirico et al. (2011) and smog chamber studies of a EURO 3 diesel passenger car (0.43 ± 0.17 , Chirico et al., 2010).

BBOA was only identified in winter 2012/2013 when it comprised 7 % of OA and summer 2013 with about 1 %. The flat diurnal of BBOA (see Fig. S16) and its correlation with the overall trend of OOA in winter suggest long-range transport of BBOA rather than regional vertical transport. A possible source region for BBOA could be Alpine valleys or the surrounding regions of the Alps where wood burning is very important in winter (Lanz et al., 2010; Herich et al., 2014; Zotter et al., 2014). During all other seasons BBOA could not be identified reliably. Even forcing a BBOA factor profile with strict constraints ($a \leq 0.05$) into the ME-2 solution always resulted in BBOA mass fractions of 1 % or less.

3.2.2 f_{44} vs. f_{43} triangle plots

Evolution of OA particles is often represented in the f_{44} vs. f_{43} space introduced by Ng et al. (2010). There, the relative contribution to total OA by the two major fragments at m/z 44 (mainly CO₂⁺) and m/z 43 (mainly C₂H₃O⁺ and C₃H₇⁺) of ambient AMS data typically fall into a triangular space indicated with red lines in Fig. 10 and temporal changes of the position up and down along the edges of the triangle can be interpreted as ageing, while changes in the horizontal direction indicate anthropogenic (biomass burning; left; traffic: left to middle) or biogenic (right) influence. The frequent injection of OA from the PBL which often experienced a different amount of ageing than the OA in the FT poses an additional important factor governing the f_{43}/f_{44} differences at the JFJ. Absolute values of f_{44} in the ACSM have to be treated with caution due to large instrument dependent variations of f_{44} found in an intercomparison of ACSM instruments by Fröhlich et al. (2015). However, the interpretations of the f_{44} vs. f_{43} triangle still hold for variations within an ACSM instrument.

In panel (a) of Fig. 10 mean f_{44} and f_{43} are shown for the full OA mass (circles) and after a subtraction of the locally emitted OA (POA_{loc}, squares), again separated by sea-

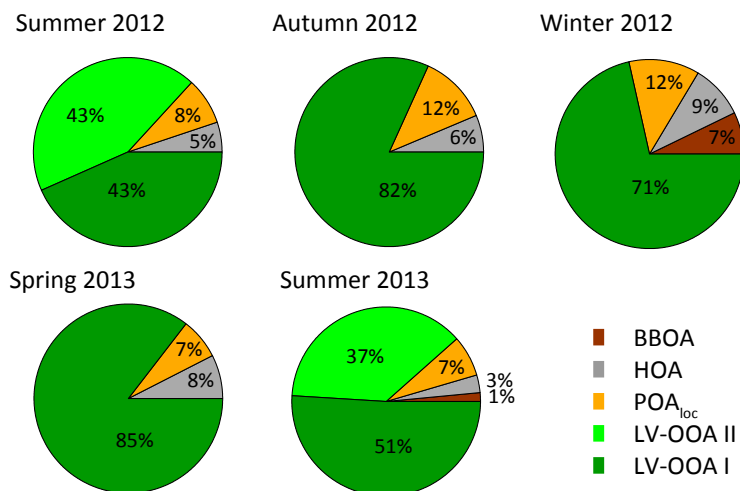


Figure 9. OA source contributions for all seasons. Orange: POA_{loc}; grey: HOA; brown: BBOA; dark green: LV-OOA I; light green: LV-OOA II.

sons. The subtraction of the fresh POA_{loc} which contains no f_{44} and about 6 % f_{43} (see Fig. S11) leads to an increase of f_{44} and a small decrease of f_{43} during all seasons, i.e. a movement in the f_{44} vs. f_{43} space towards the upper left. It is noted that a potential underestimation of f_{44} in POA_{loc} as discussed in Sect. 3.2.1 would change the shown f_{44} by less than 1 %. The overall picture, however, remains similar: in both summers a larger f_{43} was measured compared to the rest of the year indicating a mix including less aged OA with a possible predominant biogenic origin (Canonaco et al., 2015). Of the two summers, the point of summer 2012 lies more to the bottom right in the diagram than summer 2013. This is caused by a stronger contribution of vertical transport in summer 2012 compared to summer 2013 as already shown by the SA (higher LV-OOA II fraction; cf. Fig. 9) and the higher f_{43} (cf. Fig. 7). The points of autumn 2012 and spring 2013 almost lie on top of each other in the diagram, indicating similar ageing and sources. Before subtraction of POA_{loc} the autumn point showed a lower f_{44} caused by the larger amount of POA_{loc} detected compared to spring (12 vs. 7 %; cf. Fig. 9). The winter point is the only one lying on the left side of the triangle, meaning larger influence of the remaining primary sources (anthropogenic wood burning OA Heringa et al., 2011, 2012 or HOA) also after subtraction of POA_{loc}. This is justified by the increased fraction of HOA detected at the JFJ in winter compared to other seasons, which mainly originated from rare vertical transport events in winter dominating the mean values. Additionally, different importance of sources for OOA in winter (more anthropogenic) and in summer (more biogenic) may play a role (see e.g. Andreani-Aksoyoğlu et al., 2008; Hoyle et al., 2011).

Panel (b) of Fig. 10 shows the mean f_{44} and f_{43} in the presence of mainly free tropospheric air masses (white square) and during times with influence from the PBL (black

square) after the subtraction of POA_{loc}. The separation was made with the method using NO_y / CO which was described in Sect. 2.5. FT OA shows smaller f_{43} and larger f_{44} . This difference is mainly due to a higher degree of oxidation of the OOA in free tropospheric air masses consistent with the absence of sources emitting fresh OA and the longer life time of particles in the FT. Figure S13 shows a 30 % higher mass fraction of LV-OOA II to total OOA when PBL injection is happening compared to FT conditions in summer 2013.

A separation according to air mass origin (using the source area clusters described in Sect. 2.4 and displayed in Fig. 5) is shown in Fig. 10c (POA_{loc} subtracted). The very similar position of all points indicated a similar mix of OA sources from all cardinal directions. If the vertical position in Fig. 10c is interpreted as indicator for ageing, the highest degree of ageing was found in air masses from the north and south-east and the lowest degree of ageing in air masses from the west and south-west. However, the differences were small and may lie within the range of uncertainties of the methods applied. The same plot is shown in Fig. S14 after additional subtraction of the non-local POA sources identified in the ME-2 source apportionment (HOA and BBOA). The points moved up even more along the right edge of the triangle and form two clusters: a lower one containing only air masses from the west and south-west and a higher one containing the rest indicating a small difference (less oxidation) in SOA arriving from the Atlantic Ocean.

The position of only the OOA factors determined in the ME-2 analysis are shown in Fig. 10d (full OOA spectra are shown in Fig. S12 of the Supplement). For both summers LV-OOA I, LV-OOA II and the combination of both are plotted separately. Systematic variability of the degree of oxidation of OOA was observed over the course of the year. The combined OOA in summer 2012 showed the lowest f_{44} and the

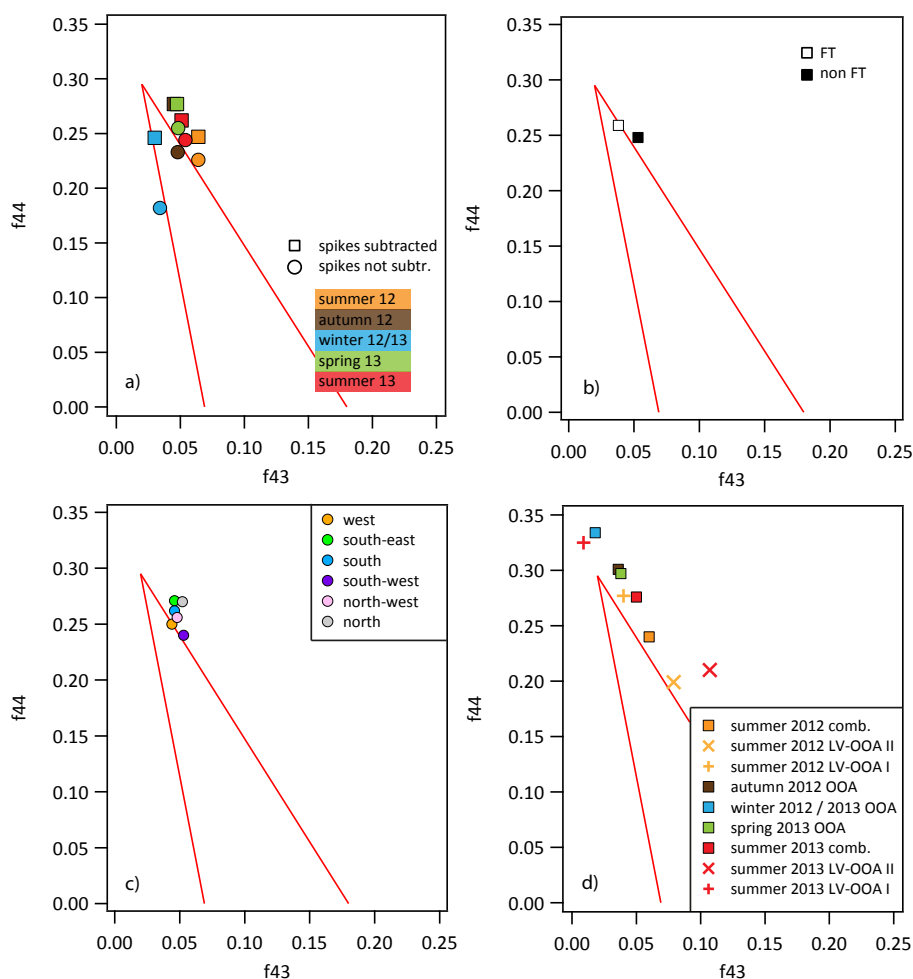


Figure 10. f_{44} vs. f_{43} plots for different boundary conditions. The triangular space in between the red lines is the region in the f_{44}/f_{43} space described by Ng et al. (2010), where atmospheric AMS data typically show up. **(a)** Separation by seasons: summer 2012 (orange), autumn 2012 (brown), winter 2012/2013 (blue), spring 2013 (green), summer 2013 (red). Circles show f_{44} and f_{43} calculated from the full data set and squares show f_{44} and f_{43} after subtraction of local OA (POA_{loc} ; see Sect. 3.2.1). **(b)** Separation by air masses (using NO_y/CO ; see Sect. 2.5): free tropospheric air masses (white square); boundary layer-influenced air masses (black square). **(c)** Separation by air mass origin (using the clusters described in Sect. 2.4 and shown in Fig. 5): west (orange), south-east (light green), south (blue), south-west (violet), north-west (pink), north (grey). **(d)** Location of OOA factors from Sect. 3.2.1 in f_{44} vs. f_{43} triangle. In summer two OOAs were found, both and the combination are shown in the plot.

highest f_{43} . The fraction of 44 increased in the colder seasons while f_{43} decreased at the same time (Canonaco et al., 2015). The points move along the right edge of the triangle indicating different degrees of oxidation. The OOAs of autumn and spring were very similar as already shown in panel (a) and the combined OOA of summer 2013 lies between summer 2012 and spring/autumn consistent with less vertical transport contribution in summer 2013 compared to summer 2012. The differences of the OOAs are mainly attributed to a difference in OA age. Vertical transport of less oxygenated OOA increases in frequency with temperature and at the JFJ transported OOA mixes with the background OOA. LV-OOA I and LV-OOA II in summer 2013 span a larger region in

the f_{44} vs. f_{43} space than in summer 2012. A reason is the imperfect overlap of both summer periods. During summer 2013 the ToF-ACSM measured during the full summer of 2013 (beginning of June to mid September), while in summer 2012 it was only measuring between the end of July and mid-September, i.e. only the late summer aerosol. A restriction of the ME-2 only to late summer 2013 resulted in a smaller range albeit that the combined OOA was still more aged (see Fig. S14).

4 Conclusions

A ToF-ACSM was operated at the Jungfraujoch Swiss site at 3580 m a.s.l. for a 14-month period spanning all meteorological seasons. A general trend of elevated PM₁ concentrations in summer, connected with increased PBL air influence due to thermally induced vertical transport and lower concentrations in winter was observed. The largest fraction (37–57 %) was comprised of organic compounds, especially in summer, while in winter and during the transient months comparably high fractions of SO₄²⁻ were measured. NO₃⁻ and NH₄⁺ contributed lower amounts. All over the year the inorganic anions were neutralised by NH₄⁺ within the measurement accuracy. The major fraction of NO₃⁻ all over the year and significant fractions of organics mainly in summer at the JFJ were imported from the PBL by regional vertical transport. In contrast, SO₄²⁻ concentrations in the FT were higher and comparable to the concentrations of the PBL injections. Similar transport effects are expected to take place all over the Alpine region, contributing to the exchange of air masses between PBL and FT. For the separation of PBL air from FT air three methods (²²²Rn, NO_y / CO and back trajectory clustering) were applied and compared, yielding similar results. This way seasonal averages of chemically speciated free tropospheric aerosol concentrations could be determined, representing the FT aerosol background over central Europe. The highly time resolved chemical composition data provide the opportunity to explore important aerosol parameters like CCN (cloud condensation nuclei) activity, which represents an important variable for the estimation of aerosol climate effects.

In addition, air masses transported to the JFJ were divided into seven origin regions by backward dispersion cluster analysis. Highest total concentrations were measured in southerly air masses (south-west to south-east) and lowest concentrations in westerly air masses from the Atlantic Ocean. Organics were dominant from all cardinal directions, but the fraction of SO₄²⁻ was significantly elevated from the south.

A closer investigation of spectral markers revealed summer maxima of *f*₄₃ and *f*₅₅, confirming the influence of vertical transport, while constant *f*₄₄ during all seasons indicated highly aged background aerosol. *f*₆₀ was increased only in winter indicating the presence of wood burning-related OA at the elevation of the JFJ.

A more detailed seasonal source apportionment using ME-2 (SoFi interface) allowed for a separation of the locally emitted OA fraction due to tourist activities (7–12 %). Comparison with highly time resolved aethalometer and CPC measurements together with a comparison of source profiles suggested cigarette smoke as main source of the local pollution. This observation indicates that increasing numbers of visitors may pose an issue for the validity of atmospheric observations at the JFJ during daytime (no local pollution was detected during the night hours when visitors are ab-

sent). Generally, the observed local pollution represents only a minor fraction of the total aerosol mass (< 5 % of NR-PM₁) and only the organic fraction is affected, i.e. it does not play a dominant role for most long-term observations performed at the JFJ. Nevertheless, if a separation is desired, the high frequency of the local pollution spikes makes it difficult to exclude all events manually. Since cigarette smoke was identified as likely source of the local pollution a smoking ban on the visitors terrace of the Sphinx research station (see sketch of Fig. S15) should be considered.

Furthermore, a small HOA fraction (3–9 %) advected to the JFJ by vertical transport with HOA / BC ratios around 1 : 2 was found. The prevailing OA source year-round however was the aged, oxygenated OOA (71–88 %) splitting up into a background LV-OOA I and a vertically transported LV-OOA II during summer. *f*₄₄ in OOA spectra decreased in the warmer seasons while *f*₄₃ increased at the same time. OOA profiles of autumn and spring showed a close similarity. BBOA was only detected in a few rare regional vertical transport events in summer 2013 and continuously during winter 2012/2013 pointing to longer-range regional transport.

The Supplement related to this article is available online at doi:10.5194/acp-15-11373-2015-supplement.

Acknowledgements. This work was supported by the Swiss Commission for Technology and Innovation, the European FP-7 project ACTRIS (grant agreement no. 262254), MeteoSwiss in the context of the Global Atmosphere Watch programme, as well as the Swiss National Science Foundation. We thank the International Foundation High Altitude Research Stations Jungfraujoch and Gornergrat (HFSJG) for the opportunity to perform experiments on the Jungfraujoch, Franz Conen from the University of Basel for providing the ²²²Rn data, and last but not least the custodians of the Research Station Joan and Martin Fischer and Maria and Urs Otz. The Swiss National Air Pollution Monitoring Network is run by Empa in collaboration with the Swiss Federal Office for the Environment. J. G. Slowik acknowledges the support of SNF Starting Grant BSSG10_155846. M. Gysel acknowledges the support of ERC grant 615922-BLACARAT.

Edited by: A. Huffman

References

- Alfarra, M. R., Coe, H., Allan, J. D., Bower, K. N., Boudries, H., Canagaratna, M. R., Jimenez, J. L., Jayne, J. T., Garforth, A. A., Li, S.-M., and Worsnop, D. R.: Characterization of urban and rural organic particulate in the Lower Fraser Valley using two Aerodyne Aerosol Mass Spectrometers, *Atmos. Environ.*, 38, 5745–5758, 2004.

- Allan, J. D., Jimenez, J. L., Williams, P. I., Alfarra, M. R., Bower, K. N., Jayne, J. T., Coe, H., and Worsnop, D. R.: Quantitative sampling using an Aerodyne aerosol mass spectrometer 1. Techniques of data interpretation and error analysis, *J. Geophys. Res.-Atmos.*, 108, 4090, doi:10.1029/2002JD002358, 2003.
- Allan, J. D., Delia, A. E., Coe, H., Bower, K. N., Alfarra, M., Jimenez, J. L., Middlebrook, A. M., Drewnick, F., Onasch, T. B., Canagaratna, M. R., Jayne, J. T., and Worsnop, D. R.: A generalised method for the extraction of chemically resolved mass spectra from Aerodyne aerosol mass spectrometer data, *J. Aerosol Sci.*, 35, 909–922, 2004.
- Andreani-Aksoyoglu, Ş., Keller, J., Alfarra, M., Prévôt, A., Sloan, J., and He, Z.: Contribution of Biogenic Emissions to Carbonaceous Aerosols in Summer and Winter in Switzerland: A Modelling Study, in: *Air Pollution Modeling and Its Application XIX*, edited by Borrego, C. and Miranda, A., NATO Science for Peace and Security Series Series C: Environmental Security, Springer Netherlands, 101–108, 2008.
- Appenzeller, C., Begert, M., Zenklusen, E., and Scherrer, S. C.: Monitoring climate at Jungfraujoch in the high Swiss Alpine region, *Sci. Total Environ.*, 391, 262–268, 2008.
- Baltensperger, U., Gäggeler, H. W., Jost, D. T., Lugauer, M., Schwikowski, M., Weingartner, E., and Seibert, P.: Aerosol climatology at the high-Alpine site Jungfraujoch, Switzerland, *J. Geophys. Res.-Atmos.*, 102, 19707–19715, 1997.
- Boucher, O., Randall, D., Artaxo, P., Bretherton, C., Feingold, G., Forster, P., Kerminen, V.-M., Kondo, Y., Liao, H., Lohmann, U., Rasch, P., Satheesh, S. K., Sherwood, S., Stevens, B., and Zhang, X. Y.: Clouds and Aerosols, in: *Climate change 2013: The physical science basis. contribution of working group I to the fifth assessment report of the intergovernmental panel on climate change*, edited by: Stocker, T., Qin, D., Plattner, G.-K., Tignor, M., Allen, S., Boschung, J., Nauels, A., Xia, Y., Bex, V., and Midgley, P. M., Cambridge University Press, Cambridge, United Kingdom and New York, NY, USA, 571–657, 2013.
- Bougiatioti, A., Stavroulas, I., Kostenidou, E., Zarnpas, P., Theodosi, C., Kouvarakis, G., Canonaco, F., Prévôt, A. S. H., Nenes, A., Pandis, S. N., and Mihalopoulos, N.: Processing of biomass-burning aerosol in the eastern Mediterranean during summertime, *Atmos. Chem. Phys.*, 14, 4793–4807, doi:10.5194/acp-14-4793-2014, 2014.
- Brown, S. G., Lee, T., Norris, G. A., Roberts, P. T., Collett Jr., J. L., Paatero, P., and Worsnop, D. R.: Receptor modeling of near-roadway aerosol mass spectrometer data in Las Vegas, Nevada, with EPA PMF, *Atmos. Chem. Phys.*, 12, 309–325, doi:10.5194/acp-12-309-2012, 2012.
- Brunner, D., Henne, S., Keller, C. A., Reimann, S., Vollmer, M. K., O'Doherty, S., and Maione, M.: An extended Kalman-filter for regional scale inverse emission estimation, *Atmos. Chem. Phys.*, 12, 3455–3478, doi:10.5194/acp-12-3455-2012, 2012.
- Budisulistiorini, S. H., Canagaratna, M. R., Croteau, P. L., Marth, W. J., Baumann, K., Edgerton, E. S., Shaw, S. L., Knipping, E. M., Worsnop, D. R., Jayne, J. T., Gold, A., and Surratt, J. D.: Real-time continuous characterization of secondary organic aerosol derived from isoprene epoxydiols in downtown Atlanta, Georgia, using the Aerodyne aerosol chemical speciation monitor, *Environ. Sci. Technol.*, 47, 5686–5694, 2013.
- Budisulistiorini, S. H., Baumann, K., Edgerton, E. S., Bairai, S. T., Mueller, S., Shaw, S. L., Knipping, E. M., Gold, A., and Surratt, J. D.: Seasonal characterization of submicron aerosol chemical composition and organic aerosol sources in the southeastern United States: Atlanta, Georgia and Look Rock, Tennessee, *Atmos. Chem. Phys. Discuss.*, 15, 22379–22417, doi:10.5194/acpd-15-22379-2015, 2015.
- Bukowiecki, N., Weingartner, E., Gysel, M., Collaud Coen, M., Zieger, P., Herrmann, E., Steinbacher, M., Gäggeler, H. W., and Baltensperger, U.: A Review of More Than 20 Years of Aerosol Observation at the High Altitude Research Station Jungfraujoch, Switzerland (3580 m asl), *Aerosol Air Qual. Res.*, doi:10.4209/aaqr.2015.05.0305, online first, 2015.
- Canagaratna, M., Jayne, J., Jimenez, J., Allan, J., Alfarra, M., Zhang, Q., Onasch, T., Drewnick, F., Coe, H., Middlebrook, A., Delia, A., Williams, L., Trimborn, A., Northway, M., DeCarlo, P., Kolb, C., Davidovits, P., and Worsnop, D.: Chemical and microphysical characterization of ambient aerosols with the Aerodyne aerosol mass spectrometer, *Mass Spectrom. Rev.*, 26, 185–222, 2007.
- Canonaco, F., Crippa, M., Slowik, J. G., Baltensperger, U., and Prévôt, A. S. H.: SoFi, an IGOR-based interface for the efficient use of the generalized multilinear engine (ME-2) for the source apportionment: ME-2 application to aerosol mass spectrometer data, *Atmos. Meas. Tech.*, 6, 3649–3661, doi:10.5194/amt-6-3649-2013, 2013.
- Canonaco, F., Slowik, J. G., Baltensperger, U., and Prévôt, A. S. H.: Seasonal differences in oxygenated organic aerosol composition: implications for emissions sources and factor analysis, *Atmos. Chem. Phys.*, 15, 6993–7002, doi:10.5194/acp-15-6993-2015, 2015.
- Carbone, S., Saarikoski, S., Frey, A., Reyes, F., Reyes, P., Castillo, M., Gramsch, E., Oyola, P., Jayne, J. T., Worsnop, D. R., and Hillamo, R.: Chemical characterization of submicron aerosol particles in Santiago de Chile, *Aerosol Air Qual. Res.*, 13, 462–473, 2013.
- Chan, K. M. and Wood, R.: The seasonal cycle of planetary boundary layer depth determined using COSMIC radio occultation data, *J. Geophys. Res.-Atmos.*, 118, 12422–12434, doi:10.1002/2013JD020147, 2013.
- Charlson, R. J., Schwartz, S. E., Hales, J. M., Cess, R. D., Coakley, J. A., Hansen, J. E., and Hofmann, D. J.: climate forcing by anthropogenic aerosols, *Science*, 255, 423–430, 1992.
- Chhabra, P. S., Flagan, R. C., and Seinfeld, J. H.: Elemental analysis of chamber organic aerosol using an aerodyne high-resolution aerosol mass spectrometer, *Atmos. Chem. Phys.*, 10, 4111–4131, doi:10.5194/acp-10-4111-2010, 2010.
- Chirico, R., DeCarlo, P. F., Heringa, M. F., Tritscher, T., Richter, R., Prévôt, A. S. H., Dommen, J., Weingartner, E., Wehrle, G., Gysel, M., Laborde, M., and Baltensperger, U.: Impact of aftertreatment devices on primary emissions and secondary organic aerosol formation potential from in-use diesel vehicles: results from smog chamber experiments, *Atmos. Chem. Phys.*, 10, 11545–11563, doi:10.5194/acp-10-11545-2010, 2010.
- Chirico, R., Prévôt, A. S., DeCarlo, P. F., Heringa, M. F., Richter, R., Weingartner, E., and Baltensperger, U.: Aerosol and trace gas vehicle emission factors measured in a tunnel using an Aerosol Mass Spectrometer and other on-line instrumentation, *Atmos. Environ.*, 45, 2182–2192, 2011.
- Cohen, A. J., Ross Anderson, H., Ostro, B., Pandey, K. D., Krzyzanowski, M., Kunzli, N., Gutschmidt, K., Pope, A.,

- Romieu, I., Samet, J. M., and Smith, K.: The global burden of disease due to outdoor air pollution, *J. Toxicol. Env. Heal. A*, 68, 1301–1307, 2005.
- Collaud Coen, M., Weingartner, E., Schaub, D., Hueglin, C., Corrigan, C., Henning, S., Schwikowski, M., and Baltensperger, U.: Saharan dust events at the Jungfraujoch: detection by wavelength dependence of the single scattering albedo and first climatology analysis, *Atmos. Chem. Phys.*, 4, 2465–2480, doi:10.5194/acp-4-2465-2004, 2004.
- Collaud Coen, M., Weingartner, E., Nyeki, S., Cozic, J., Henning, S., Verheggen, B., Gehrig, R., and Baltensperger, U.: Long-term trend analysis of aerosol variables at the high-Alpine site Jungfraujoch, *J. Geophys. Res.-Atmos.*, 112, D13213, doi:10.1029/2006jd007995, 2007.
- Cozic, J., Verheggen, B., Weingartner, E., Crosier, J., Bower, K. N., Flynn, M., Coe, H., Henning, S., Steinbacher, M., Henne, S., Collaud Coen, M., Petzold, A., and Baltensperger, U.: Chemical composition of free tropospheric aerosol for PM₁ and coarse mode at the high alpine site Jungfraujoch, *Atmos. Chem. Phys.*, 8, 407–423, doi:10.5194/acp-8-407-2008, 2008.
- Crippa, M., DeCarlo, P. F., Slowik, J. G., Mohr, C., Heringa, M. F., Chirico, R., Poulain, L., Freutel, F., Sciare, J., Cozic, J., Di Marco, C. F., Elsasser, M., Nicolas, J. B., Marchand, N., Abidi, E., Wiedensohler, A., Drewnick, F., Schneider, J., Borrmann, S., Nemitz, E., Zimmermann, R., Jaffrezo, J.-L., Prévôt, A. S. H., and Baltensperger, U.: Wintertime aerosol chemical composition and source apportionment of the organic fraction in the metropolitan area of Paris, *Atmos. Chem. Phys.*, 13, 961–981, doi:10.5194/acp-13-961-2013, 2013.
- Crippa, M., Canonaco, F., Lanz, V. A., Äijälä, M., Allan, J. D., Carbone, S., Capes, G., Ceburnis, D., Dall'Osto, M., Day, D. A., DeCarlo, P. F., Ehn, M., Eriksson, A., Freney, E., Hildebrandt Ruiz, L., Hillamo, R., Jimenez, J. L., Junninen, H., Kiendler-Scharr, A., Kortelainen, A.-M., Kulmala, M., Laaksonen, A., Mensah, A. A., Mohr, C., Nemitz, E., O'Dowd, C., Ovadnevaite, J., Pandis, S. N., Petäjä, T., Poulain, L., Saarikoski, S., Sellegri, K., Swietlicki, E., Tiitta, P., Worsnop, D. R., Baltensperger, U., and Prévôt, A. S. H.: Organic aerosol components derived from 25 AMS data sets across Europe using a consistent ME-2 based source apportionment approach, *Atmos. Chem. Phys.*, 14, 6159–6176, doi:10.5194/acp-14-6159-2014, 2014.
- Cross, E. S., Slowik, J. G., Davidovits, P., Allan, J. D., Worsnop, D. R., Jayne, J. T., Lewis, D. K., Canagaratna, M., and Onasch, T. B.: Laboratory and ambient particle density determinations using light scattering in conjunction with aerosol mass spectrometry, *Aerosol Sci. Tech.*, 41, 343–359, 2007.
- Cubison, M. J., Ortega, A. M., Hayes, P. L., Farmer, D. K., Day, D., Lechner, M. J., Brune, W. H., Apel, E., Diskin, G. S., Fisher, J. A., Fuelberg, H. E., Hecobian, A., Knapp, D. J., Mikoviny, T., Riemer, D., Sachse, G. W., Sessions, W., Weber, R. J., Weinheimer, A. J., Wisthaler, A., and Jimenez, J. L.: Effects of aging on organic aerosol from open biomass burning smoke in aircraft and laboratory studies, *Atmos. Chem. Phys.*, 11, 12049–12064, doi:10.5194/acp-11-12049-2011, 2011.
- Faber, P., Drewnick, F., Veres, P. R., Williams, J., and Borrmann, S.: Anthropogenic sources of aerosol particles in a football stadium: Real-time characterization of emissions from cigarette smoking, cooking, hand flares, and color smoke bombs by high-resolution aerosol mass spectrometry, *Atmos. Environ.*, 77, 1043–1051, 2013.
- Forrer, J., Rüttimann, R., Schneiter, D., Fischer, A., Buchmann, B., and Hofer, P.: Variability of trace gases at the high-Alpine site Jungfraujoch caused by meteorological transport processes, *J. Geophys. Res.-Atmos.*, 105, 12241–12251, doi:10.1029/1999JD901178, 2000.
- Freney, E. J., Sellegri, K., Canonaco, F., Boulon, J., Hervé, M., Weigel, R., Pichon, J. M., Colomb, A., Prévôt, A. S. H., and Laj, P.: Seasonal variations in aerosol particle composition at the puy-de-Dôme research station in France, *Atmos. Chem. Phys.*, 11, 13047–13059, doi:10.5194/acp-11-13047-2011, 2011.
- Fröhlich, R., Cubison, M. J., Slowik, J. G., Bukowiecki, N., Prévôt, A. S. H., Baltensperger, U., Schneider, J., Kimmel, J. R., Gonin, M., Rohner, U., Worsnop, D. R., and Jayne, J. T.: The ToF-ACSM: a portable aerosol chemical speciation monitor with TOFMS detection, *Atmos. Meas. Tech.*, 6, 3225–3241, doi:10.5194/amt-6-3225-2013, 2013.
- Fröhlich, R., Crenn, V., Setyan, A., Belis, C. A., Canonaco, F., Favez, O., Riffault, V., Slowik, J. G., Aas, W., Äijälä, M., Alastuey, A., Artijano, B., Bonnaire, N., Bozzetti, C., Bressi, M., Carbone, C., Coz, E., Croteau, P. L., Cubison, M. J., Esser-Giel, J. K., Green, D. C., Gros, V., Heikkinen, L., Herrmann, H., Jayne, J. T., Lunder, C. R., Minguillón, M. C., Mocnik, G., O'Dowd, C. D., Ovadnevaite, J., Petralia, E., Poulain, L., Priestman, M., Ripoll, A., Sarda-Estève, R., Wiedensohler, A., Baltensperger, U., Sciare, J., and Prévôt, A. S. H.: ACTRIS ACSM intercomparison – Part 2: Intercomparison of ME-2 organic source apportionment results from 15 individual, co-located aerosol mass spectrometers, *Atmos. Meas. Tech.*, 8, 2555–2576, doi:10.5194/amt-8-2555-2015, 2015.
- Galasyn, J. F., Tschudy, K. L., and Huebert, B. J.: Seasonal and diurnal variability of nitric acid vapor and ionic aerosol species in the remote free troposphere at Mauna Loa, Hawaii, *J. Geophys. Res.-Atmos.*, 92, 3105–3113, doi:10.1029/JD092iD03p03105, 1987.
- Griffiths, A. D., Conen, F., Weingartner, E., Zimmermann, L., Chambers, S. D., Williams, A. G., and Steinbacher, M.: Surface-to-mountaintop transport characterised by radon observations at the Jungfraujoch, *Atmos. Chem. Phys.*, 14, 12763–12779, doi:10.5194/acp-14-12763-2014, 2014.
- Guo, H., Xu, L., Bougiatioti, A., Cerully, K. M., Capps, S. L., Hite Jr., J. R., Carlton, A. G., Lee, S.-H., Bergin, M. H., Ng, N. L., Nenes, A., and Weber, R. J.: Fine-particle water and pH in the southeastern United States, *Atmos. Chem. Phys.*, 15, 5211–5228, doi:10.5194/acp-15-5211-2015, 2015.
- Hammer, E., Bukowiecki, N., Gysel, M., Jurányi, Z., Hoyle, C. R., Vogt, R., Baltensperger, U., and Weingartner, E.: Investigation of the effective peak supersaturation for liquid-phase clouds at the high-alpine site Jungfraujoch, Switzerland (3580 m a.s.l.), *Atmos. Chem. Phys.*, 14, 1123–1139, doi:10.5194/acp-14-1123-2014, 2014.
- Hansen, A.: The aethalometer, Magee Scientific Company, Berkeley, CA, 2005.
- Henne, S., Furger, M., Nyeki, S., Steinbacher, M., Neining, B., de Wekker, S. F. J., Dommen, J., Spichtinger, N., Stohl, A., and Prévôt, A. S. H.: Quantification of topographic venting of boundary layer air to the free troposphere, *Atmos. Chem. Phys.*, 4, 497–509, doi:10.5194/acp-4-497-2004, 2004.

- Henne, S., Furger, M., and Prévôt, A. H.: Climatology of mountain venting-induced elevated moisture layers in the lee of the Alps, *J. Appl. Meteorol.*, 44, 620–633, 2005.
- Henne, S., Brunner, D., Folini, D., Solberg, S., Klausen, J., and Buchmann, B.: Assessment of parameters describing representativeness of air quality in-situ measurement sites, *Atmos. Chem. Phys.*, 10, 3561–3581, doi:10.5194/acp-10-3561-2010, 2010.
- Hennigan, C. J., Izumi, J., Sullivan, A. P., Weber, R. J., and Nenes, A.: A critical evaluation of proxy methods used to estimate the acidity of atmospheric particles, *Atmos. Chem. Phys.*, 15, 2775–2790, doi:10.5194/acp-15-2775-2015, 2015.
- Henning, S., Weingartner, E., Schwikowski, M., Gäggeler, H. W., Gehrig, R., Hinz, K.-P., Trimborn, A., Spengler, B., and Baltensperger, U.: Seasonal variation of water-soluble ions of the aerosol at the high-Alpine site Jungfraujoch (3580 m asl), *J. Geophys. Res.-Atmos.*, 108, ACH8.1–ACH8.10, doi:10.1029/2002JD002439, 2003.
- Herich, H., Kammermann, L., Gysel, M., Weingartner, E., Baltensperger, U., Lohmann, U., and Cziczo, D. J.: In situ determination of atmospheric aerosol composition as a function of hygroscopic growth, *J. Geophys. Res.-Atmos.*, 113, D16213, doi:10.1029/2008JD009954, 2008.
- Herich, H., Gianini, M., Piot, C., Močnik, G., Jaffrezo, J.-L., Besombes, J.-L., Prévôt, A., and Hueglin, C.: Overview of the impact of wood burning emissions on carbonaceous aerosols and PM in large parts of the Alpine region, *Atmos. Environ.*, 89, 64–75, 2014.
- Heringa, M. F., DeCarlo, P. F., Chirico, R., Tritscher, T., Dommen, J., Weingartner, E., Richter, R., Wehrle, G., Prévôt, A. S. H., and Baltensperger, U.: Investigations of primary and secondary particulate matter of different wood combustion appliances with a high-resolution time-of-flight aerosol mass spectrometer, *Atmos. Chem. Phys.*, 11, 5945–5957, doi:10.5194/acp-11-5945-2011, 2011.
- Heringa, M. F., DeCarlo, P. F., Chirico, R., Lauber, A., Doberer, A., Good, J., Nussbaumer, T., Keller, A., Burtscher, H., Richard, A., Miljevic, B., Prevot, A. S. H., and Baltensperger, U.: Time-resolved characterization of primary emissions from residential wood combustion appliances, *Environ. Sci. Technol.*, 46, 11418–11425, 2012.
- Herrmann, E., Gysel, M., Weingartner, E., Bukowiecki, N., Hammer, E., Jurányi, Z., Collaud Coen, M., Vuilleumier, L., Steinbacher, M., Henne, S., Conen, F., and Baltensperger, U.: What shapes the aerosol size distribution at high altitudes? – Longterm observations from Jungfraujoch, *J. Geophys. Res.-Atmos.*, 120, doi:10.1002/2015JD023660, online first, 2015.
- Hildebrandt, L., Engelhart, G. J., Mohr, C., Kostenidou, E., Lanz, V. A., Bougiatioti, A., DeCarlo, P. F., Prevot, A. S. H., Baltensperger, U., Mihalopoulos, N., Donahue, N. M., and Pandis, S. N.: Aged organic aerosol in the Eastern Mediterranean: the Finokalia Aerosol Measurement Experiment – 2008, *Atmos. Chem. Phys.*, 10, 4167–4186, doi:10.5194/acp-10-4167-2010, 2010.
- Hildemann, L. M., Markowski, G. R., and Cass, G. R.: Chemical composition of emissions from urban sources of fine organic aerosol, *Environ. Sci. Tech.*, 25, 744–759, 1991.
- Hoyle, C. R., Boy, M., Donahue, N. M., Fry, J. L., Glasius, M., Guenther, A., Hallar, A. G., Huff Hartz, K., Petters, M. D., Petäjä, T., Rosenoern, T., and Sullivan, A. P.: A review of the anthropogenic influence on biogenic secondary organic aerosol, *Atmos. Chem. Phys.*, 11, 321–343, doi:10.5194/acp-11-321-2011, 2011.
- Jaeglé, L., Jacob, D. J., Wang, Y., Weinheimer, A. J., Ridley, B. A., Campos, T. L., Sachse, G. W., and Hagen, D. E.: Sources and chemistry of NO_x in the upper troposphere over the United States, *Geophys. Res. Lett.*, 25, 1705–1708, doi:10.1029/97GL03591, 1998.
- Jayne, J., Leard, D., Zhang, X., Davidovits, P., Smith, K., Kolb, C., and Worsnop, D.: Development of an aerosol mass spectrometer for size and composition analysis of submicron particles, *Aerosol Sci. Tech.*, 33, 49–70, 2000.
- Jimenez, J. L., Canagaratna, M. R., Donahue, N. M., Prévôt, A. S. H., Zhang, Q., Kroll, J. H., DeCarlo, P. F., Allan, J. D., Coe, H., Ng, N. L., Aiken, A. C., Docherty, K. S., Ulbrich, I. M., Grieshop, A. P., Robinson, A. L., Duplissy, J., Smith, J. D., Wilson, K. R., Lanz, V. A., Hueglin, C., Sun, Y. L., Tian, J., Laaksonen, A., Raatikainen, T., Rautiainen, J., Vaattovaara, P., Ehn, M., Kulmala, M., Tomlinson, J. M., Collins, D. R., Cubison, M. J., E., Dunlea, J., Huffman, J. A., Onasch, T. B., Alfarra, M. R., Williams, P. I., Bower, K., Kondo, Y., Schneider, J., Drewnick, F., Borrmann, S., Weimer, S., Demerjian, K., Salcedo, D., Cottrell, L., Griffin, R., Takami, A., Miyoshi, T., Hatakeyama, S., Shimojo, A., Sun, J. Y., Zhang, Y. M., Dzepina, K., Kimmel, J. R., Sueper, D., Jayne, J. T., Herndon, S. C., Trimborn, A. M., Williams, L. R., Wood, E. C., Middlebrook, A. M., Kolb, C. E., Baltensperger, U., and Worsnop, D. R.: Evolution of organic aerosols in the atmosphere, *Science*, 326, 1525–1529, 2009.
- Jurányi, Z., Gysel, M., Weingartner, E., DeCarlo, P. F., Kammermann, L., and Baltensperger, U.: Measured and modelled cloud condensation nuclei number concentration at the high alpine site Jungfraujoch, *Atmos. Chem. Phys.*, 10, 7891–7906, doi:10.5194/acp-10-7891-2010, 2010.
- Jurányi, Z., Gysel, M., Weingartner, E., Bukowiecki, N., Kammermann, L., and Baltensperger, U.: A 17 month climatology of the cloud condensation nuclei number concentration at the high alpine site Jungfraujoch, *J. Geophys. Res.-Atmos.*, 116, D10204, doi:10.1029/2010jd015199, 2011.
- Keller, C. A., Brunner, D., Henne, S., Vollmer, M. K., O'Doherty, S., and Reimann, S.: Evidence for under-reported western European emissions of the potent greenhouse gas HFC-23, *Geophys. Res. Lett.*, 38, L15808, doi:10.1029/2011GL047976, 2011.
- Kleeman, M. J., Schauer, J. J., and Cass, G. R.: Size and composition distribution of fine particulate matter emitted from wood burning, meat charbroiling, and cigarettes, *Environ. Sci. Tech.*, 33, 3516–3523, 1999.
- Laden, F., Neas, L. M., Dockery, D. W., and Schwartz, J.: Association of fine particulate matter from different sources with daily mortality in six U.S. cities, *Environ. Health Persp.*, 108, 941–947, 2000.
- Lanz, V. A., Alfarra, M. R., Baltensperger, U., Buchmann, B., Hueglin, C., and Prévôt, A. S. H.: Source apportionment of submicron organic aerosols at an urban site by factor analytical modelling of aerosol mass spectra, *Atmos. Chem. Phys.*, 7, 1503–1522, doi:10.5194/acp-7-1503-2007, 2007.
- Lanz, V. A., Alfarra, M. R., Baltensperger, U., Buchmann, B., Hueglin, C., Szidat, S., Wehrli, M. N., Wacker, L., Weimer, S., Caseiro, A., Puxbaum, H., and Prevot, A. S. H.: Source attribution of submicron organic aerosols during wintertime inversions

- by advanced factor analysis of aerosol mass spectra, *Environ. Sci. Tech.*, 42, 214–220, 2008.
- Lanz, V. A., Prévôt, A. S. H., Alfarra, M. R., Weimer, S., Mohr, C., DeCarlo, P. F., Gianini, M. F. D., Hueglin, C., Schneider, J., Favez, O., D'Anna, B., George, C., and Baltensperger, U.: Characterization of aerosol chemical composition with aerosol mass spectrometry in Central Europe: an overview, *Atmos. Chem. Phys.*, 10, 10453–10471, doi:10.5194/acp-10-10453-2010, 2010.
- Lee, C., Martin, R. V., van Donkelaar, A., Lee, H., Dickerson, R. R., Hains, J. C., Krotkov, N., Richter, A., Vinnikov, K., and Schwab, J. J.: SO₂ emissions and lifetimes: Estimates from inverse modeling using in situ and global, space-based (SCIAMACHY and OMI) observations, *J. Geophys. Res.-Atmos.*, 116, D06304, doi:10.1029/2010JD014758, 2011.
- Lohmann, U. and Feichter, J.: Global indirect aerosol effects: a review, *Atmos. Chem. Phys.*, 5, 715–737, doi:10.5194/acp-5-715-2005, 2005.
- Lugauer, M., Baltensperger, U., Furger, M., Gäggeler, H., Jost, D., Schwikowski, M., and Wanner, H.: Aerosol transport to the high Alpine sites Jungfraujoch (3454 m asl) and Colle Gnifetti (4452 m asl), *Tellus B*, 50, 76–92, doi:10.3402/tellusb.v50i1.16026, 1998.
- Mahowald, N.: Aerosol indirect effect on biogeochemical cycles and climate, *Science*, 334, 794–796, 2011.
- Matthew, B. M., Middlebrook, A. M., and Onasch, T. B.: Collection efficiencies in an Aerodyne aerosol mass spectrometer as a function of particle phase for laboratory generated aerosols, *Aerosol Sci. Tech.*, 42, 884–898, 2008.
- Minguillón, M. C., Ripoll, A., Pérez, N., Prévôt, A. S. H., Canonaco, F., Querol, X., and Alastuey, A.: Chemical characterization of submicron regional background aerosols in the western Mediterranean using an Aerosol Chemical Speciation Monitor, *Atmos. Chem. Phys.*, 15, 6379–6391, doi:10.5194/acp-15-6379-2015, 2015.
- Mohr, C., Huffman, J. A., Cubison, M. J., Aiken, A. C., Docherty, K. S., Kimmel, J. R., Ulbrich, I. M., Hannigan, M., and Jimenez, J. L.: Characterization of Primary Organic Aerosol Emissions from Meat Cooking, Trash Burning, and Motor Vehicles with High-Resolution Aerosol Mass Spectrometry and Comparison with Ambient and Chamber Observations, *Environ. Sci. Technol.*, 43, 2443–2449, 2009.
- Mohr, C., DeCarlo, P. F., Heringa, M. F., Chirico, R., Slowik, J. G., Richter, R., Reche, C., Alastuey, A., Querol, X., Seco, R., Peñuelas, J., Jiménez, J. L., Crippa, M., Zimmermann, R., Baltensperger, U., and Prévôt, A. S. H.: Identification and quantification of organic aerosol from cooking and other sources in Barcelona using aerosol mass spectrometer data, *Atmos. Chem. Phys.*, 12, 1649–1665, doi:10.5194/acp-12-1649-2012, 2012.
- Morrical, B. D. and Zenobi, R.: Detection of polycyclic aromatic compounds at Jungfraujoch high-Alpine research station using two-step laser mass spectrometry, *Int. J. Environ. An. Ch.*, 82, 377–385, 2002.
- Ng, N. L., Canagaratna, M. R., Zhang, Q., Jimenez, J. L., Tian, J., Ulbrich, I. M., Kroll, J. H., Docherty, K. S., Chhabra, P. S., Bahreini, R., Murphy, S. M., Seinfeld, J. H., Hildebrandt, L., Donahue, N. M., DeCarlo, P. F., Lanz, V. A., Prévôt, A. S. H., Dinar, E., Rudich, Y., and Worsnop, D. R.: Organic aerosol components observed in Northern Hemispheric datasets from Aerosol Mass Spectrometry, *Atmos. Chem. Phys.*, 10, 4625–4641, doi:10.5194/acp-10-4625-2010, 2010.
- Ng, N. L., Canagaratna, M. R., Jimenez, J. L., Chhabra, P. S., Seinfeld, J. H., and Worsnop, D. R.: Changes in organic aerosol composition with aging inferred from aerosol mass spectra, *Atmos. Chem. Phys.*, 11, 6465–6474, doi:10.5194/acp-11-6465-2011, 2011a.
- Ng, N. L., Canagaratna, M. R., Jimenez, J. L., Zhang, Q., Ulbrich, I. M., and Worsnop, D. R.: Real-time methods for estimating organic component mass concentrations from aerosol mass spectrometer data, *Environ. Sci. Technol.*, 45, 910–916, 2011b.
- Ng, N. L., Herndon, S. C., Trimborn, A., Canagaratna, M. R., Croteau, P. L., Onasch, T. B., Sueper, D., Worsnop, D. R., Zhang, Q., Sun, Y. L., and Jayne, J. T.: An aerosol chemical speciation monitor (ACSM) for routine monitoring of the composition and mass concentrations of ambient aerosol, *Aerosol Sci. Tech.*, 45, 780–794, 2011c.
- Northway, M. J., Jayne, J. T., Toohey, D. W., Canagaratna, M. R., Trimborn, A., Akiyama, K. I., Shimono, A., Jimenez, J. L., DeCarlo, P. F., Wilson, K. R., and Worsnop, D. R.: Demonstration of a VUV lamp photoionization source for improved organic speciation in an aerosol mass spectrometer, *Aerosol Sci. Tech.*, 41, 828–839, 2007.
- Nyeki, S., Kalberer, M., Colbeck, I., De Wekker, S., Furger, M., Gäggeler, H. W., Kossmann, M., Lugauer, M., Steyn, D., Weingartner, E., Wirth, M., and Baltensperger, U.: Convective boundary layer evolution to 4 km asl over high-Alpine terrain: Airborne lidar observations in the Alps, *Geophys. Res. Lett.*, 27, 689–692, doi:10.1029/1999GL010928, 2000.
- Ovadnevaite, J., Ceburnis, D., Leinert, S., Dall'Osto, M., Canagaratna, M., O'Doherty, S., Berresheim, H., and O'Dowd, C.: Submicron NE Atlantic marine aerosol chemical composition and abundance: Seasonal trends and air mass categorization, *J. Geophys. Res.-Atmos.*, 119, 11850–11863, 2014.
- Paatero, P.: Least squares formulation of robust non-negative factor analysis, *Chemometr. Intell. Lab.*, 37, 23–35, 1997.
- Paatero, P.: The multilinear engine – a table-driven, least squares program for solving multilinear problems, including the n-way parallel factor analysis model, *J. Comput. Graph. Stat.*, 8, 854–888, 1999.
- Paatero, P. and Hopke, P. K.: Rotational tools for factor analytic models, *J. Chemometrics*, 23, 91–100, 2009.
- Paatero, P. and Tapper, U.: Positive matrix factorization: a non-negative factor model with optimal utilization of error estimates of data values, *Environmetrics*, 5, 111–126, 1994.
- Pandey Deolal, S., Brunner, D., Steinbacher, M., Weers, U., and Staehelin, J.: Long-term in situ measurements of NO_x and NO_y at Jungfraujoch 1998–2009: time series analysis and evaluation, *Atmos. Chem. Phys.*, 12, 2551–2566, doi:10.5194/acp-12-2551-2012, 2012.
- Pandey Deolal, S., Staehelin, J., Brunner, D., Cui, J., Steinbacher, M., Zellweger, C., Henne, S., and Vollmer, M. K.: Transport of PAN and NO_y from different source regions to the Swiss high alpine site Jungfraujoch, *Atmos. Environ.*, 64, 103–115, doi:10.1016/j.atmosenv.2012.08.021, 2013.
- Pandey Deolal, S., Henne, S., Ries, L., Gilge, S., Weers, U., Steinbacher, M., Staehelin, J., and Peter, T.: Analysis of elevated springtime levels of Peroxyacetyl nitrate (PAN) at the high

- Alpine research sites Jungfraujoch and Zugspitze, *Atmos. Chem. Phys.*, 14, 12553–12571, doi:10.5194/acp-14-12553-2014, 2014.
- Parworth, C., Fast, J., Mei, F., Shippert, T., Sivaraman, C., Tilp, A., Watson, T., and Zhang, Q.: Long-term measurements of submicrometer aerosol chemistry at the Southern Great Plains (SGP) using an Aerosol Chemical Speciation Monitor (ACSM), *Atmos. Environ.*, 106, 43–55, 2015.
- Petit, J.-E., Favez, O., Sciare, J., Crenn, V., Sarda-Estève, R., Bonnaire, N., Mocnik, G., Dupont, J.-C., Haeffelin, M., and Leoz-Garziandia, E.: Two years of near real-time chemical composition of submicron aerosols in the region of Paris using an Aerosol Chemical Speciation Monitor (ACSM) and a multi-wavelength Aethalometer, *Atmos. Chem. Phys.*, 15, 2985–3005, doi:10.5194/acp-15-2985-2015, 2015.
- Pfaffenberger, L., Barnet, P., Slowik, J. G., Praplan, A. P., Dommen, J., Prévôt, A. S. H., and Baltensperger, U.: The link between organic aerosol mass loading and degree of oxygenation: an α -pinene photooxidation study, *Atmos. Chem. Phys.*, 13, 6493–6506, doi:10.5194/acp-13-6493-2013, 2013.
- Pope, C. A. and Dockery, D. W.: Health effects of fine particulate air pollution: lines that connect, *J. Air Waste Manage.*, 56, 709–742, 2006.
- Preunkert, S., Wagenbach, D., and Legrand, M.: Improvement and characterization of an automatic aerosol sampler for remote (glacier) sites, *Atmos. Environ.*, 36, 1221–1232, 2002.
- Ramanathan, V., Crutzen, P. J., Kiehl, J. T., and Rosenfeld, D.: Aerosols, climate, and the hydrological cycle, *Science*, 294, 2119–2124, 2001.
- Reimann, S., Vollmer, M., Folini, D., Steinbacher, M., Hill, M., Buchmann, B., Zander, R., and Mahieu, E.: Observations of long-lived anthropogenic halocarbons at the high-Alpine site of Jungfraujoch (Switzerland) for assessment of trends and European sources, *Sci. Total Environ.*, 391, 224–231, research at Jungfraujoch – Contributions to the International conference in celebration of the 75th anniversary of the High Altitude Research Station Jungfraujoch at Interlaken, Switzerland, 11–13 September, 2006, 2008.
- Ripoll, A., Minguillón, M. C., Pey, J., Jimenez, J. L., Day, D. A., Sosedova, Y., Canonaco, F., Prévôt, A. S. H., Querol, X., and Alastuey, A.: Long-term real-time chemical characterization of submicron aerosols at Montsec (southern Pyrenees, 1570 m a.s.l.), *Atmos. Chem. Phys.*, 15, 2935–2951, doi:10.5194/acp-15-2935-2015, 2015.
- Rotach, M. W. and Zardi, D.: On the boundary-layer structure over highly complex terrain: Key findings from MAP, *Q. J. Roy. Meteor. Soc.*, 133, 937–948, doi:10.1002/qj.71, 2007.
- Schwikowski, M., Seibert, P., Baltensperger, U., and Gaggeler, H.: A study of an outstanding Saharan dust event at the high-Alpine site Jungfraujoch, Switzerland, *Atmos. Environ.*, 29, 1829–1842, doi:10.1016/1352-2310(95)00060-C, 1995.
- Seaton, A., Godden, D., MacNee, W., and Donaldson, K.: Particulate air pollution and acute health effects, *Lancet*, 345, 176–178, 1995.
- Seidel, D. J., Ao, C. O., and Li, K.: Estimating climatological planetary boundary layer heights from radiosonde observations: Comparison of methods and uncertainty analysis, *J. Geophys. Res.-Atmos.*, 115, D16113, doi:10.1029/2009JD013680, 2010.
- Shindell, D. and Faluvegi, G.: Climate response to regional radiative forcing during the twentieth century, *Nat. Geosci.*, 2, 294–300, 2009.
- Shrestha, A. B., Wake, C. P., and Dibb, J. E.: Chemical composition of aerosol and snow in the high Himalaya during the summer monsoon season, *Atmos. Environ.*, 31, 2815–2826, doi:10.1016/S1352-2310(97)00047-2, 1997.
- Stohl, A., Trainer, M., Ryerson, T. B., Holloway, J. S., and Parrish, D. D.: Export of NO_y from the North American boundary layer during 1996 and 1997 North Atlantic Regional Experiments, *J. Geophys. Res.-Atmos.*, 107, ACH11.1–ACH11.13, doi:10.1029/2001JD000519, 2002.
- Stohl, A., Forster, C., Frank, A., Seibert, P., and Wotawa, G.: Technical note: The Lagrangian particle dispersion model FLEXPART version 6.2, *Atmos. Chem. Phys.*, 5, 2461–2474, doi:10.5194/acp-5-2461-2005, 2005.
- Stott, P. A.: Attribution of regional-scale temperature changes to anthropogenic and natural causes, *Geophys. Res. Lett.*, 30, 1724, doi:10.1029/2003GL017324, 2003.
- Sturm, P., Tuzson, B., Henne, S., and Emmenegger, L.: Tracking isotopic signatures of CO₂ at the high altitude site Jungfraujoch with laser spectroscopy: analytical improvements and representative results, *Atmos. Meas. Tech.*, 6, 1659–1671, doi:10.5194/amt-6-1659-2013, 2013.
- Sun, Y., Wang, Z., Dong, H., Yang, T., Li, J., Pan, X., Chen, P., and Jayne, J. T.: Characterization of summer organic and inorganic aerosols in Beijing, China with an Aerosol Chemical Speciation Monitor, *Atmos. Environ.*, 51, 250–259, 2012.
- Takahama, S., Johnson, A., Morales, J. G., Russell, L., Duran, R., Rodriguez, G., Zheng, J., Zhang, R., Toom-Saunty, D., and Leaitch, W.: Submicron organic aerosol in Tijuana, Mexico, from local and Southern California sources during the CalMex campaign, *Atmos. Environ.*, 70, 500–512, 2013.
- Tang, X., Zheng, Z., Jung, H. S., and Asa-Awuku, A.: The effects of mainstream and sidestream environmental tobacco smoke composition for enhanced condensational droplet growth by water vapor, *Aerosol Sci. Tech.*, 46, 760–766, 2012.
- Tiitta, P., Vakkari, V., Croteau, P., Beukes, J. P., van Zyl, P. G., Josipovic, M., Venter, A. D., Jaars, K., Pienaar, J. J., Ng, N. L., Canagaratna, M. R., Jayne, J. T., Kerminen, V.-M., Kokkola, H., Kulmala, M., Laaksonen, A., Worsnop, D. R., and Laakso, L.: Chemical composition, main sources and temporal variability of PM₁ aerosols in southern African grassland, *Atmos. Chem. Phys.*, 14, 1909–1927, doi:10.5194/acp-14-1909-2014, 2014.
- Uglietti, C., Leuenberger, M., and Brunner, D.: European source and sink areas of CO₂ retrieved from Lagrangian transport model interpretation of combined O₂ and CO₂ measurements at the high alpine research station Jungfraujoch, *Atmos. Chem. Phys.*, 11, 8017–8036, doi:10.5194/acp-11-8017-2011, 2011.
- Ulbrich, I. M., Canagaratna, M. R., Zhang, Q., Worsnop, D. R., and Jimenez, J. L.: Interpretation of organic components from Positive Matrix Factorization of aerosol mass spectrometric data, *Atmos. Chem. Phys.*, 9, 2891–2918, doi:10.5194/acp-9-2891-2009, 2009.
- Vakkari, V., Kerminen, V.-M., Beukes, J. P., Tiitta, P., van Zyl, P. G., Josipovic, M., Venter, A. D., Jaars, K., Worsnop, D. R., Kulmala, M., and Laakso, L.: Rapid changes in biomass burning aerosols by atmospheric oxidation, *Geophys. Res. Lett.*, 41, 2644–2651, 2014.

- van Donkelaar, A., Martin, R. V., Brauer, M., Kahn, R., Levy, R., Verduzco, C., and Villeneuve, P. J.: Global estimates of ambient fine particulate matter concentrations from satellite-based aerosol optical depth: development and application, *Environ. Health Perspect.*, 118, 847–855, 2010.
- Watson, J. G., Robinson, N. F., Lewis, C., Coulter, T., Chow, J. C., Fujita, E. M., Lowenthal, D., Conner, T. L., Henry, R. C., and Willis, R. D.: Chemical mass balance receptor model version 8 (CMB8) user's manual, Prepared for US Environmental Protection Agency, Research Triangle Park, NC, by Desert Research Institute, Reno, NV, 1997.
- Weingartner, E., Nyeki, S., and Baltensperger, U.: Seasonal and diurnal variation of aerosol size distributions ($10 < D < 750$ nm) at a high-Alpine site (Jungfraujoch 3580 m asl), *J. Geophys. Res.-Atmos.*, 104, 26809–26820, doi:10.1029/1999JD900170, 1999.
- Weingartner, E., Saathoff, H., Schnaiter, M., Streit, N., Bitnar, B., and Baltensperger, U.: Absorption of light by soot particles: determination of the absorption coefficient by means of aethalometers, *J. Aerosol Sci.*, 34, 1445–1463, 2003.
- Weissmann, M., Braun, F., Gantner, L., Mayr, G., Rahm, S., and Reitebuch, O.: The Alpine mountain-plain circulation: Airborne Doppler lidar measurements and numerical simulations, *Mon. Weather Rev.*, 133, 3095–3109, 2005.
- Yamazawa, H., Miyazaki, T., Moriizumi, J., Iida, T., Takeda, S., Nagara, S., Sato, K., and Tokizawa, T.: Radon exhalation from a ground surface during a cold snow season, *Int. Congr. Ser.*, 1276, 221–222, doi:10.1016/j.ics.2004.11.153, 2005.
- Young, D. E., Allan, J. D., Williams, P. I., Green, D. C., Flynn, M. J., Harrison, R. M., Yin, J., Gallagher, M. W., and Coe, H.: Investigating the annual behaviour of submicron secondary inorganic and organic aerosols in London, *Atmos. Chem. Phys.*, 15, 6351–6366, doi:10.5194/acp-15-6351-2015, 2015.
- Zanatta, M., Gysel, M., Bukowiecki, N., Weingartner, E., Baltensperger, U., Cavalli, F., Areskoug, A., Fiebig, M., Kouvarakis, G., Beddows, D., Putaud, J.-P., Spindler, G., Wiedensohler, A., Pandolfi, M., Alastuey, A., Müller, D., Swietlicki, E., Laj, P., and Sellegri, K.: *Atmos. Chem. Phys. Discuss.*, in preparation, 2015.
- Zander, R., Mahieu, E., Demoulin, P., Duchatelet, P., Roland, G., Servais, C., Mazière, M. D., Reimann, S., and Rinsland, C.: Our changing atmosphere: Evidence based on long-term infrared solar observations at the Jungfraujoch since 1950, *Sci. Total Environ.*, 391, 184–195, 2008.
- Zellweger, C., Forrer, J., Hofer, P., Nyeki, S., Schwarzenbach, B., Weingartner, E., Ammann, M., and Baltensperger, U.: Partitioning of reactive nitrogen (NO_y) and dependence on meteorological conditions in the lower free troposphere, *Atmos. Chem. Phys.*, 3, 779–796, doi:10.5194/acp-3-779-2003, 2003.
- Zellweger, C., Steinbacher, M., and Buchmann, B.: Evaluation of new laser spectrometer techniques for in-situ carbon monoxide measurements, *Atmos. Meas. Tech.*, 5, 2555–2567, doi:10.5194/amt-5-2555-2012, 2012.
- Zhang, Q., Worsnop, D. R., Canagaratna, M. R., and Jimenez, J. L.: Hydrocarbon-like and oxygenated organic aerosols in Pittsburgh: insights into sources and processes of organic aerosols, *Atmos. Chem. Phys.*, 5, 3289–3311, doi:10.5194/acp-5-3289-2005, 2005.
- Zhang, Q., Jimenez, J. L., Canagaratna, M. R., Allan, J. D., Coe, H., Ulbrich, I., Alfarra, M. R., Takami, A., Middlebrook, A. M., Sun, Y. L., Dzepina, K., Dunlea, E., Docherty, K., DeCarlo, P. F., Salcedo, D., Onasch, T., Jayne, J. T., Miyoshi, T., Shimono, A., Hatakeyama, S., Takegawa, N., Kondo, Y., Schneider, J., Drewnick, F., Borrmann, S., Weimer, S., Demerjian, K., Williams, P., Bower, K., Bahreini, R., Cottrell, L., Griffin, R. J., Rautiainen, J., Sun, J. Y., Zhang, Y. M., and Worsnop, D. R.: Ubiquity and dominance of oxygenated species in organic aerosols in anthropogenically-influenced Northern Hemisphere midlatitudes, *Geophys. Res. Lett.*, 34, L13801, doi:10.1029/2007GL029979, 2007.
- Zhang, Q., Jimenez, J. L., Canagaratna, M. R., Ulbrich, I. M., Ng, N. L., Worsnop, D. R., and Sun, Y.: Understanding atmospheric organic aerosols via factor analysis of aerosol mass spectrometry: a review, *Anal. Bioanal. Chem.*, 401, 3045–3067, 2011.
- Zotter, P., Ciobanu, V. G., Zhang, Y. L., El-Haddad, I., Macchia, M., Daellenbach, K. R., Salazar, G. A., Huang, R.-J., Wacker, L., Hueglin, C., Piazzalunga, A., Fermo, P., Schwikowski, M., Baltensperger, U., Szidat, S., and Prévôt, A. S. H.: Radiocarbon analysis of elemental and organic carbon in Switzerland during winter-smog episodes from 2008 to 2012 – Part 1: Source apportionment and spatial variability, *Atmos. Chem. Phys.*, 14, 13551–13570, doi:10.5194/acp-14-13551-2014, 2014.